

PREDICTED FE II EMISSION-LINE STRENGTHS FROM ACTIVE GALACTIC NUCLEI

T. A. A. SIGUT

Department of Physics and Astronomy, The University of Western Ontario

AND

ANIL K. PRADHAN

Department of Astronomy, The Ohio State University

Submitted to The Astrophysical Journal Supplement Series

ABSTRACT

We present theoretical Fe II emission line strengths for physical conditions typical of Active Galactic Nuclei with Broad-Line Regions. The Fe II line strengths were computed with a precise treatment of radiative transfer using extensive and accurate atomic data from the Iron Project. Excitation mechanisms for the Fe II emission included continuum fluorescence, collisional excitation, self-fluorescence among the Fe II transitions, and fluorescent excitation by Ly α and Ly β . A large Fe II atomic model consisting of 827 fine structure levels (including states to $E \approx 15$ eV) was used to predict fluxes for approximately 23,000 Fe II transitions, covering most of the UV, optical, and IR wavelengths of astrophysical interest. Spectral synthesis for wavelengths from $\lambda 1600 \text{ \AA}$ to $1.2 \mu\text{m}$ is presented. Applications of present theoretical templates to the analysis of observations are described. In particular, we discuss recent observations of near-IR Fe II lines in the 8500 \AA – $1 \mu\text{m}$ region which are predicted by the Ly α fluorescence mechanism. We also compare our UV spectral synthesis with an empirical iron template for the prototypical, narrow-line Seyfert galaxy I Zw 1. The theoretical Fe II template presented in this work should also be applicable to a variety of objects with Fe II spectra formed under similar excitation conditions, such as supernovae and symbiotic stars.

Subject headings: quasars: emission lines — line: formation — line: identification — Supernova

1. INTRODUCTION

Transitions of singly ionized iron dominate the spectra of many astrophysical objects, from the sun and stars to active galactic nuclei (AGNs) and quasars (Viotti 1988). However, the interpretation of this spectrum is complex, and to extract meaningful results for the physical conditions in the emitting region, and the iron abundance and ionization fractions, one is faced with the solution of a complex radiative transfer problem requiring the specification of many thousands of radiative and collisional rates in a non-local thermodynamic equilibrium (non-LTE) formalism. Until recently, such calculations have been hampered by the paucity of basic atomic data for Fe II. However, the Iron Project (Hummer *et al.* 1993) has been specifically initiated to address this problem, and new, accurate atomic data for Fe II have been calculated. In particular, radiative dipole transition probabilities for over 21,000 fine-structure transitions of Fe II have been computed by Nahar (1995), and collision strengths for over 11,000 fine-structure transitions have been computed by Zhang & Pradhan (1995) and Bautista & Pradhan (1996). These calculations, and the Iron Project in general, employ the powerful and accurate R-matrix method (Burke & Berrington 1993).

In our earlier work on Fe II (Sigut & Pradhan 1998; SP98), we employed a limited, non-LTE atomic model with 262 fine structure levels which was still sufficiently large for Ly α fluorescent excitation to be investigated in detail. It was shown that Ly α excitation can be of fundamental importance in enhancing the UV and optical Fe II fluxes. In particular, it was predicted that

Ly α fluorescence results in significant near-infrared Fe II emission in the region $\lambda\lambda 8500$ – 9500 \AA . Following the SP98 work, recent observations have detected many of these near-IR Fe II emission lines from several narrow-line Seyfert I galaxies (Rodriguez-Ardila *et al.* 2001), and from a Type IIn supernova remnant with narrow emission lines (Fransson *et al.* 2001). Although difficult to observe, these near-IR Fe II lines should be indicative of the excitation mechanisms and the possible interplay between collisional and fluorescent excitation (Rudy *et al.* 2000). As our predicted near-IR Fe II fluxes in this wavelength region are likely to be of wider interest, this paper presents a detailed line list from our non-LTE calculations with an extended Fe II model atom.

We intend this line list to be our first step in developing a reliable set of *theoretical* templates for the iron emission from AGN. Currently, due to the complexity of the observed iron emission from AGN, such emission is typically modeled using empirical templates derived from specific AGN spectra (Boroson & Green 1992, Corbin & Boroson 1996). A recent example of this method is the Fe II–Fe III template of Vestergaard & Wilkes (2001) derived from high-quality UV spectra of the narrow-line Seyfert I galaxy I Zw 1. Such templates play a critical role in extracting a measure of the total iron emission from heavily blended and broadened AGN spectra. For example, Dietrich *et al.* (2002) apply the Vestergaard & Wilkes template to extract a measure of the relative iron-to-magnesium abundance ratio from a sample of high- z quasars. Such studies seek to constrain the epoch of major star formation in AGN using the iron-to-magnesium abundance ratio

as a nucleosynthesis “clock” following Hamann & Ferland (1992). Such studies are beginning to impose important cosmological constraints: for example, Aoki, Murayama & Denda (2002) have detected Fe II emission from a $z = 5.74$ QSO with a strength comparable to much lower redshift objects.

Empirical templates have the advantage that they can side-step the complicated process of specifying in detail the iron emission mechanisms, and have generally found to provide better fits to observations than theoretical templates (Iwamuro *et al.* 2002, Thompson, Hill & Elston 1999). Nevertheless, there is still a strong need to develop reliable theoretical templates: (1) empirical templates assume that the underlying AGN population used to construct the template is typical and that the iron emission in other related objects can be modeled as a simple scaling of the fiducial spectrum. (2) Empirical templates can never be completely free of the complications introduced by the large blending and broadening present in AGN spectra. For example, it is difficult to constrain the iron emission present at the location of the Mg II h & k lines, although such an estimate does affect the derived fluxes.

Theoretical iron flux templates can address both of these problems, allowing estimates of the response of the iron emission to model parameters which may differ from object to object (such as the photoionizing radiation field), and providing a spectrum from which complex blended features can be decomposed into their individual contributions. But theoretical templates must first show that they can explain the current empirical templates. In this work, we will compare our predictions with the empirical UV template of Vestergaard & Wilkes.

1.1. The Physics of Fe II Line Formation in AGN

The formation of the Fe II emission spectrum from AGN is still poorly understood (Joly 1993, Hamann & Ferland 1999). Typically, photoionization cloud models for the BLR fail to account for the observed strength of the Fe II emission. A class of “super-strong” Fe II emitters is known (Lipari, Macchetto & Golombek 1991; Graham *et al.* 1996) which seem to be unaccountable by traditional photoionized models. In these cases, and possibly all, a different cloud population may be the origin of the Fe II emission, such as mechanically heated clouds shielded from the central continuum source (Joly 1987), perhaps originating in the outer regions of an accretion disk (Collin-Souffrin *et al.* 1988). An important sub-class of AGN with BLRs are the narrow-line Seyfert galaxies (Osterbrock & Pogge 1985). I Zw 1 is the prototypical narrow-line quasar (Laor *et al.* 1997), and it is also a strong Fe II emitter (Marziani *et al.* 1996). Such narrow-line Seyfert 1 galaxies (NLS1) enable both better emission line diagnostics and better tests of theoretical spectra as their spectra are broadened with typical velocities of $\leq 1000 \text{ km s}^{-1}$.

The accepted micro-physics of Fe II line formation in AGN is that of Wills, Netzer & Wills (1985) with the extension by Elitzur & Netzer (1985) to include fluorescent excitation by Ly α . The Ly α excitation process is further studied by Johansson & Jordan (1984), Penston (1987), Sigut & Pradhan (1998), and Verner *et al.* (1999). The proposed excitation mechanisms can be understood with the aid of the highly simplified Fe II energy level dia-

gram shown in Fig. 1, based on a similar figure by Penston (1987). Four principal excitation mechanisms have been included:

(1) **CONTINUUM FLUORESCENCE:** Photons incident on the illuminated face of the BLR cloud are absorbed in the resonance transitions and are subsequently re-radiated in the resonance and optical lines. Strong optical emission, however, requires thermalization of the resonance transitions in order to shift the effective branching ratio towards optical emission. Thus this mechanism suffers from having the photon source in the wrong location, namely outside the cloud at small optical depth, something first noted by Netzer (1988).

(2) **COLLISIONAL EXCITATION:** Inelastic collisions with electrons excite the odd parity levels near 5 eV which then decay into the optical and UV lines. This mechanism is efficient whenever the gas temperature is above $\approx 7000 \text{ K}$, temperatures which are generally found in photoionized models of the BLR. Excitation is irrespective of the local optical depth in the Fe II lines, and thus this mechanism does not suffer the limitations of continuum fluorescence. It is generally believed that collisional excitation is responsible for the bulk of the Fe II emission.

(3) **SELF-FLUORESCENCE:** Netzer & Wills (1983) suggested that self-fluorescence, that is absorption of the Fe II UV resonance photons by overlapping UV Fe II transitions originating from the odd parity levels near 5 eV (labeled “unexpected UV” in Fig. 1) was an important source of excitation to highly excited states due to the large number of wavelength coincidences between these groupings of levels.

(4) **FLUORESCENT EXCITATION BY Ly α :** Penston (1987) noted that, despite theoretical calculations to the contrary (Elitzur & Netzer 1985), there is indirect evidence that Ly α fluorescence may be an important but overlooked excitation mechanism. Penston noted the presence of unexpected UV Fe II lines (see Fig. 1) in the spectrum of the symbiotic star RR Tel that seemed attributable only to cascades from higher levels pumped by Ly α fluorescence. The emission nebulae of symbiotics offer densities and ionization parameters similar to those inferred for the BLRs of AGN. Graham *et al.* (1996) have identified emission from the UV Fe II multiplets expected to be preferentially strengthened by this mechanism, as noted by Penston, in the spectrum of the ultra-strong Fe II emitter 2226-3905.

In this current work, in addition to considerably enlarging the Fe II atomic model to 827 fine structure levels up to $E \approx 15 \text{ eV}$, we make improvements to the modeling of all of these excitation mechanisms:

(1) We solve the equation of radiative transfer with continuum fluorescence included through the appropriate boundary conditions on the transfer equations.

(2) We use a large and accurate set of R-matrix collision strengths for electron impact excitation of Fe II. Such rates are available for many of the key odd parity levels near 5 eV with are the upper levels of most of the UV and optical emission.

(3) Line-overlap among the Fe II transitions is included exactly in the radiative transfer solutions. We considerably expand the Fe II atomic model to 827 fine-structure levels and over 23,000 radiative transitions.

(4) We include frequency-dependent source functions for Ly α and Ly β in the monochromatic source functions used in the radiative transfer solutions. While the Ly α and Ly β source functions used are approximate, as discussed in the Section 3.1, their inclusion into the radiative transfer solution is exact.

2. THE ATOMIC DATA

The non-LTE calculations require a considerable amount of atomic data, not only for Fe II but also for several nearby ionization stages. Fe I - Fe IV were considered in the calculation, with Fe I, Fe III, and Fe IV represented as one level atoms with ground state photoionization cross sections and total radiative-plus-dielectronic recombination rates adopted from the Ohio-State group calculations (<http://www.astronomy.ohio-state.edu/~pradhan>; Bautista & Pradhan 1995; Nahar *et al.* 1997; Nahar 1996; Nahar 1996; Bautista & Pradhan 1997; Nahar & Bautista 1999). The Fe II atomic model consisted of 827 fine-structure levels representing the 265 $LS\pi$ multiplets with observed energies (Johansson 1978). An extensive Fe II atom is necessary for realistic estimates of the total emitted flux (Wills, Netzer & Wills 1985). Rates between fine-structure levels, as opposed to total $LS\pi$ terms, were used to make straightforward the inclusion of line-overlap among the Fe II transitions themselves and fluorescent excitation by Ly α and Ly β . The doublet, quartet, and sextet spin systems are illustrated in Figure 2 (as well as the Ly α fluorescence paths); a few octet terms (a^8S^e , z^8P^o , a^8P^e , and a^8D^e) were included in the calculation but are not shown in this Figure.

Radiative transition probabilities for Fe II were drawn from three sources: the critical compilation of Fuhr, Martin & Wiese (1988), the R-matrix calculations for dipole-allowed transitions ($\Delta S = 0$) of Nahar (1995), and the extensive semi-empirical calculations of Kurucz (1991, private communication). In total, these sources give about 23,000 fine-structure transitions between the included energy levels which satisfy $f_{ij} > 10^{-4}$ and $\lambda_{ij} < 3 \mu\text{m}$.

Photoionization cross sections for all Fe II levels were adopted from Nahar (1996), who computed them with the R-matrix method and also employed a unified treatment of radiative and dielectronic recombination. The full resonance structure of these cross sections was retained. A state-specific radiative-plus-dielectronic recombination coefficient was used for each Fe II quartet and sextet level. The remaining levels included only radiative recombination through the Milne relation. Stimulated recombination was also included, but generally makes a negligible contribution to the total recombination rates.

For collisional excitation of Fe II by electron impact, we adopt the R-matrix results of Zhang & Pradhan (1995, denoted ZP) and Bautista & Pradhan (1996, denoted BP). The ZP calculation utilized a 38-state close coupling target for Fe II, mainly representing the quartet and sextet symmetries of the $3d^6 4s$, $3d^7$, and $3d^6 4p$ configurations. This calculation provides collisional excitation rates to many of the key odd-parity levels between 5 and 7 eV which are the upper levels of the resonance and optical Fe II emission lines. The BP calculation used a somewhat different target expansion designed to give collision strengths for transitions among the low-lying even parity levels, including

the doublet system. Collision strengths for electron excitation of all remaining dipole-allowed transitions were computed with the effective Gaunt factor approximation of Van Regemorter (1969) with a Gaunt factor of 0.3. Collisional coupling by electron excitation of the fine-structure levels of each $LS\pi$ multiplet not explicitly computed by ZP or BP were estimated by assuming that the highest energy set of fine-structure collision strengths in each $LS\pi$ symmetry computed by ZP or BP could be used as estimates for the fine-structure rates within all higher $LS\pi$ multiplets. If ZP or BP rates were unavailable for any members in an $LS\pi$ symmetry, the fine-structure collision strengths were set to 2.0 for $\Delta J = 0, \pm 1$, and 0.5 otherwise.

Charge transfer recombination rates to Fe II - Fe IV were adopted from Kingdon & Ferland (1996). Charge transfer ionization of Fe II was also included because recombination from Fe III is to the Fe II ground state (Neufeld & Dalgarno 1987). All of these charge transfer rates were computed in the Landau-Zener approximation (see Flower 1990 for a discussion of this method), and hence are not of the same accuracy as most of the atomic data used in this work. We also note that the large rates predicted by this method for the iron ions results in the domination of the charge-transfer reactions in determining the iron ionization balance in AGN BLR clouds.

3. CALCULATIONS FOR FE II FLUXES

The coupled equations of radiative transfer and statistical equilibrium were solved with the accelerated lambda-iteration method of Rybicki & Hummer (1991, 1992). As overlap between the Fe II transitions is extensive and complex, the full preconditioning strategy suggested by Rybicki & Hummer (1992) was implemented. A diagonal approximate lambda operator was used because of the large size of the iron atomic model. Complete frequency redistribution (CRD) over depth-dependent Doppler profiles was assumed for all of the Fe II radiative transitions. The width of the Doppler profile for each transition was assumed to be

$$\Delta\nu_D = \frac{\nu}{c} \left(\frac{2kT_e}{m} + \zeta_t^2 \right)^{\frac{1}{2}}, \quad (1)$$

where ζ_t is the internal microturbulent velocity in the BLR clouds.

In order to solve the radiative transfer and statistical equilibrium equations, it is necessary to know the structure of the BLR clouds, that is the run of T_e and N_e , the photoionizing radiation field, and the background continuous opacities and source functions. To obtain these quantities, we used the CLOUDY code of Ferland (1991). The cloud structure was fixed during the iron non-LTE calculation. The CLOUDY models are traditional plane-parallel, one dimensional, power-law illuminated clouds computed for a single ionization parameter and total particle density, assuming constant total pressure. The shape of the photoionizing continuum incident on the cloud was taken from Mathews & Ferland (1987). The particle conservation equation, which closes the system of statistical equilibrium equations, was written at each depth as

$$\sum_{i=1}^N n_i = N_H \epsilon_{Fe} \left(\sum_{j=1}^4 f_j \right), \quad (2)$$

where N_H is the total hydrogen number density, ϵ_{Fe} is the iron abundance relative to hydrogen, and f_j is the fraction of ionization stage j of iron as predicted by CLOUDY. The solar iron abundance is $\log(N_{Fe}/N_H) = -4.52$.

3.1. Fluorescent Excitation and Radiative Transfer

$\text{Ly}\alpha$ pumping of the Fe II emission was included by first computing the frequency dependence of the $\text{Ly}\alpha$ line emissivity. As stimulated emission is not important, the emission profile for this process can be set equal to the absorption profile without significant error, and with this approximation, the frequency-dependent $\text{Ly}\alpha$ source function can be written as

$$S_\nu^{Ly\alpha} = \left(\frac{n_{2p} A_{2p,1s}}{n_{1s} B_{1s,2p} - n_{2p} B_{2p,1s}} \right) \frac{\psi_\nu}{\phi_\nu}. \quad (3)$$

The quantity in brackets is the frequency-independent source function valid for complete redistribution. The absorption profile, ϕ_ν , was taken to be a depth-dependent Voigt profile with a damping width set by natural broadening. The emission profile, ψ_ν , complicates the problem considerably as it, in general, depends on the radiation field (Mihalas 1978). We have retained the CLOUDY estimates of the $1s$ and $2p$ H I level populations in eq. (3), but have explicitly computed the emission profile using the redistribution function

$$R(\nu', \nu) = \gamma_c R_{II}(\nu', \nu) + (1 - \gamma_c) \phi_{\nu'} \phi_\nu. \quad (4)$$

Here γ_c is the fraction of coherently scattered photons in the atom's rest frame. Our treatment of the redistribution function for resonance line emission, $R_{II}(\nu', \nu)$, follows Venerazz, Avrett & Loeser (1981) by using the partial coherent scattering (PCS) approximation in a form suggested by Kneer (1975),

$$R_{II}(\nu', \nu) \approx \langle a \rangle_\nu \phi_{\nu'} \delta(\nu' - \nu) + (1 - a_{\nu' \nu}) \phi_{\nu'} \phi_\nu. \quad (5)$$

Here the function $a_{\nu' \nu}$ effects the transition from complete redistribution in the core to coherent scattering in the wings, and

$$\langle a \rangle_{\nu' \nu} = \int a_{\nu' \nu} \phi_{\nu'} d\nu'. \quad (6)$$

The relation between $a_{\nu' \nu}$ and $\langle a \rangle_\nu$ ensures the correct normalization of the redistribution function. We have used the form of $a_{\nu' \nu}$ described by Venerazz, Avrett & Loeser (1981).

In the PCS approximation, the ratio of the emission to absorption profile can be written as

$$\frac{\psi_\nu}{\phi_\nu} = 1 + \gamma_c \left(\frac{\langle a \rangle_\nu J_\nu - \langle aJ \rangle_\nu}{\bar{J}} \right), \quad (7)$$

where

$$\langle aJ \rangle_\nu = \int a_{\nu' \nu} \phi_{\nu'} J_{\nu'} d\nu', \quad (8)$$

and

$$\bar{J} = \int \phi_{\nu'} J_{\nu'} d\nu'. \quad (9)$$

The main limitation of the PCS approximation is that it fails to account for Doppler diffusion in the coherent wings (Basri 1980). However, given the other approximations made in this work, the use of the exact redistribution function seems unwarranted. We have verified our treatment by matching the $\text{Ly}\alpha$ profiles tabulated for BLR clouds by

Avrett & Loeser (1988) using their models and hydrogen populations (see Figure 3). We have tried both values of γ_c suggested by Avrett & Loeser (1988), 0.998, the best theoretical estimate, and 0.98, which gives the best match to the solar profile. For all calculations, the $\text{Ly}\alpha$ source function was calculated independently and held fixed during the Fe II solution.

$\text{Ly}\beta$ was included in exactly the same manner as $\text{Ly}\alpha$, except that the fraction of coherent scattering was assumed to be 0.4. The $n = 1$ and 3 level populations were also adopted from the CLOUDY model.

In the radiative transfer solutions, fluorescent excitation by Fe II line overlap and by $\text{Ly}\alpha$ (or $\text{Ly}\beta$ with analogous expressions) was included by constructing the total monochromatic source function at each frequency as

$$S_\nu = \sum_l \frac{\chi_\nu^l}{\chi_\nu} S^l + \frac{\chi_\nu^c}{\chi_\nu} S^{bck} + \frac{\chi_\nu^{Ly\alpha}}{\chi_\nu} S_\nu^{Ly\alpha}, \quad (10)$$

where S^l is the CRD line source function for each contributing iron transition, S^{bck} is the background continuum source function, and $S_\nu^{Ly\alpha}$ is the $\text{Ly}\alpha$ frequency-dependent PRD source function. The total monochromatic opacity at frequency ν is given by

$$\chi_\nu = \sum_l \chi_\nu^l + \chi_\nu^c + \chi_\nu^{Ly\alpha}. \quad (11)$$

where χ_ν^l is the opacity due to each contributing iron transition, χ_ν^c is the background continuous opacity, and $\chi_\nu^{Ly\alpha}$ is the opacity due $\text{Ly}\alpha$. The $\text{Ly}\alpha$ source function and opacity were not assumed to be constant across the iron line profiles. Table 1 lists the Fe II transitions originating from a^4D^e within ± 3 Å of $\text{Ly}\alpha$. Critical parameters in the strength of this pumping are the oscillator strengths of the Fe II transitions. As shown in the Table, the recent results of Nahar (1996) and Kurucz (1991, private communication) generally estimate oscillator strengths about an order of magnitude larger than Kurucz (1981).

The total line flux in each Fe II transition was computed with two methods: First, as frequency-angle dependent radiative transfer is explicitly solved, the fluxes can be computed from the emergent line profiles, relative to the continuum, just as in the analysis of observations,

$$F_{ji} = \int_{\Delta\nu_{ij}} (F_\nu^i - F_c^i) d\nu + \int_{\Delta\nu_{ij}} (F_\nu^s - F_c^s) d\nu. \quad (12)$$

Here, $\Delta\nu_{ij}$ is the integration bandwidth for the $i - j$ transition, and F_c is the continuum flux at the line's frequency. The first term is the emission from the illuminated face, and the second, the emission from the shielded face.

Another way of computing the emergent flux is from the cooling function. Considering *only* the line $i - j$, the first moment of the transfer equation integrated over frequency gives

$$\frac{dF_{ji}^o}{dz} = 4\pi \int_{\Delta\nu} \chi_\nu^l (S^l - J_\nu) d\nu. \quad (13)$$

This clearly represents the cooling (or heating) due to the $i - j$ transition in $\text{ergs cm}^{-3} \text{s}^{-1}$. Substituting for the line opacity and the line source function in terms of the level populations, and defining the *net radiative bracket* for the transition $i - j$ as

$$\rho_{ij} \equiv 1 - \frac{\bar{J}_{ij}}{\bar{S}^l}, \quad (14)$$

we have

$$\frac{dF_{ji}^o}{dz} = h\nu A_{ji} n_j \rho_{ij} \equiv \Phi_{ij}(z). \quad (15)$$

Thus we can define a net line flux escaping from both sides of the cloud as the integral of the cooling function over depth

$$F_{ij}^o \equiv \int \Phi_{ij}(z) dz. \quad (16)$$

This is a very convenient expression for the flux and provides the most direct connection between the flux predicted by exact radiative transfer and traditional escape probability methods. In the later case, an escape probability function replaces the net radiative bracket. However, it is important to realize that $F_{ji}^o \neq F_{ji}$, as the latter is defined as the flux relative to the continuum, in the absence of the line. Performing a similar analysis for the continuum alone, it is trivial to show that the relation between these two fluxes is

$$F_{ji} = F_{ij}^o + 4\pi \int_{\Delta\nu_{ij}} (\chi_\nu^c - \sigma_\nu) (J_\nu^c - J_\nu) d\nu. \quad (17)$$

Here, J_ν^c is the mean intensity in the continuum in the absence of the line.

Generally, both equations (12) and (17) have been used to compute the emergent fluxes in the lines. As these two methods compute the fluxes in very different ways, agreement between the two methods is a good check on the consistency of the calculation (Avrett & Loeser 1988). Agreement in the current work was generally within few percent.

4. RESULTS AND DISCUSSION

Fe II spectra were computed for four BLR cloud models typical of the conditions thought to exist in the Fe II emitting clouds. The calculations have been made for traditional clouds of a single specified density and ionization parameter, as opposed to the more realistic *locally optimally emitting* cloud models of Baldwin *et al.* (1995), as the main interest of the current work is the interplay of the various iron emission excitation mechanisms and not the detailed structure of the BLR. Table 2 lists the basic BLR parameters, along with the total $H\beta$ flux predicted by CLOUDY which is used to normalize the total Fe II flux of Figure 4. For each basic cloud model, several values of the cloud's internal turbulent velocity (0, 10, 20 and 40 km s^{-1}) and iron abundance (1/3 solar, solar, and 3 times solar) were adopted. Detailed tabular fluxes and spectral-synthesis plots are presented for one of these models, model A, for a calculation including both $\text{Ly}\alpha$ and $\text{Ly}\beta$ fluorescent excitation. Predicted fluxes for the 600 strongest Fe II transitions are given in Table 3, and Figures 7 to 11 show the predicted Fe II spectrum. Two spectra are shown, one broadened by convolution with a dispersion profile with a width of 100 km s^{-1} , and one broadened by 500 km s^{-1} ; these atypically low broadenings are selected for clarity, with 500 km s^{-1} approaching the lowest observed values for AGN (*e.g.* 1 Zw I) and 100 km s^{-1} appropriate for the "nano-quasars" (accreting white dwarfs) of Zamanov & Marziani (2002). The BLR clouds were assumed to have a covering fraction of 5% of the central continuum source with equal contributions from the illuminated and shielded cloud faces.

The predicted Fe II fluxes from these models generally cover most of ultraviolet (UV), optical (Opt), and infrared (IR) wavelengths of interest in astrophysical sources. While the line fluxes from the present non-LTE models are particular to the assumed BLR conditions of AGNs, similar excitation mechanisms and conditions may prevail in other sources, such as symbiotic stars and supernova. In such cases, the Fe II line list of Table 3 should be useful in the identification of observed features or the absence thereof. The line fluxes given in Table 3 utilize a model atom which is considerably larger than previous works. For example, Verner *et al.* (1999) consider 371 levels, up to 11.59 eV, partially using the Iron Project data described in section 2. Also their radiative transfer treatment is approximate, employing escape probability methods, which, while being easier, may not be sufficiently precise for an accurate treatment of the strong $\text{Ly}\alpha$ excitation of Fe II.

The dependence of the total predicted UV+Opt Fe II flux, relative to $H\beta$, on the internal microturbulence (ζ_t), the total iron abundance (ϵ_{Fe}), and the inclusion or exclusion of $\text{Ly}\alpha$ and $\text{Ly}\beta$ fluorescent excitation, is shown in Figure 4 for each of the models of Table 2. When looking at the trend with abundance, it should be kept in mind that the predicted net Fe II cooling has not been used to recompute the CLOUDY BLR model; thus, the trends are likely overestimates of the real effect because of the strong "thermostatic" effect of the Fe II cooling. These figures clearly show the importance of $\text{Ly}\alpha$ fluorescent excitation on the Fe II fluxes. The influence of $\text{Ly}\alpha$ is largest for the higher ionization parameter, $U_{\text{ion}} = 10^{-2}$, and for the lower particle density, $\log(N_H) = 9.6$; the higher particle density tends to thermalize the $\text{Ly}\alpha$ source function which reduces the net pumping rate. The total predicted Fe II flux, relative to $H\beta$, is largest for the lower ionization parameter models, $U_{\text{ion}} = 10^{-3}$, and the lowest density, $\log(N_H) = 9.6$. The assumed internal cloud microturbulent velocity, a poorly known parameter, is also seen to have a large impact on the predicted fluxes at higher abundances. To extract realistic abundances for the BLR, a clear procedure needs to be developed to constrain this parameter.

The distribution of Fe II fluxes in model A with and without $\text{Ly}\alpha$ fluorescent excitation is illustrated in Figure 5. The upper-left panel shows the cumulative predicted flux, including $\text{Ly}\alpha$ and $\text{Ly}\beta$ pumping, as the Fe II fluxes are summed from the strongest to weakest transition. The 50% point occurs after only the 120 strongest transitions, whereas the 90% point is reached after 1250 transitions. The figure also shows that the cumulative flux distribution is reasonably well fit by a function of the form

$$F(n) = \sum_{i=1}^n F_i = F_{\text{tot}} \left(1 - e^{-(n/N_o)^\alpha} \right) \quad (18)$$

with $\alpha \approx 0.53$ and $N_o \approx 240$. Here F_{tot} is the total Fe II flux. The bottom-left panel shows a histogram of the actual distribution in the \log_{10} of the Fe II fluxes; the distribution is seen to be double-peaked which is a consequence of $\text{Ly}\alpha$ fluorescent excitation. The rightmost panels of Figure 5 illustrate the case excluding $\text{Ly}\alpha$ fluorescent excitation. In this case, roughly half the number of transitions are required to carry 50%, and 90% of the total flux, namely 50 and 625 transitions respectively, and the

flux distribution is no longer double-peaked. The best-fit parameters of Equation 18 for the cumulative flux distribution are $\alpha \approx 0.48$ and $N_o \approx 107$.

An alternative view of the Fe II flux distribution is given in Figure 6. This Figure shows a histogram of the predicted Fe II flux, including Ly α and Ly β pumping, based on the energy of the upper level of each transition. Again, two peaks in the distribution can be seen, one near $0.4 - 0.5$ Ryd where the flux originates from lines collisionally excited from the ground configurations to the low-lying, odd-parity levels, and a second one at higher energies corresponding to the initial cascades from Ly α pumping. The lower panel shows a histogram of the number of Fe II energy levels as a function of energy. Again, BLR model A was employed for these calculations.

4.1. Theoretical Templates

The predicted line fluxes, such as those of Table 3 may serve as the basis for a set of theoretical templates for the Fe II emission from AGN covering the entire wavelength region from the UV to the near-IR. Subsets of these templates may be used to study individual Fe II features or to subtract the total contribution of Fe II in a particular range. Sample subsets of the UV line fluxes in the $1600 - 3100$ Å region are shown in Figures 7, 8, and 9, a region which contains among the strongest Fe II emission features.

Figure 12 compares our predicted UV fluxes with the empirical Fe II-Fe III template of Vestergaard & Wilkes (2001). The underlying cloud model used for the calculation is model B of Table 2, which was found to give the best fit among the four models. The calculated spectrum was convolved with a dispersion profile of a width of 900 km s^{-1} and then normalized to the average relative flux of the observed template spectrum in the range of $\lambda 2400-2500$ Å. The figure shows the computed spectrum both with, and without, fluorescent excitation for several combinations of the internal cloud microturbulence (ζ_t) and iron abundance (ϵ_{Fe}). A strong constraint on the model fits is the flatness of the observed UV emission between 2300 and 2600 Å. Overall, the observed spectrum can be reproduced in broad outline, although many individual features remain discrepant. However, we are not trying to propose a specific BLR model for I Zw 1, but simply to compare its Fe II spectrum to the current predictions of our BLR models. Another UV comparison with I Zw 1 is shown in Fig. 13. Here, the computed Fe II template in the interesting $1500 - 2200$ Å wavelength range is compared to observations of Marziani *et al.* 1996. Several of the UV features (albeit blended) correspond well to the observed ones, thus facilitating identification and determination of lines from Fe II and other ionic species.

Our predicted optical and IR line fluxes are shown in Figures 10 and 11, covering wavelengths from 3100 Å to $1.2 \mu\text{m}$. These lines may be resolved through high-resolution spectroscopy and can provide useful plasma diagnostics of the emitting regions. The optical/IR lines can be divided into two groups: those from among the low-lying levels of Fe II which depend primarily on the electron temperature and density, and those from among the high-lying levels which are populated primarily by cascades from upper levels and are therefore dependent on

fluorescent excitation and ($e^- + \text{Fe III}$) recombination. Because the atomic physics considerations are different, one may distinguish between the two groups through correlations between the observed and theoretical spectra, as discussed in the next section.

4.2. Fluorescent Excitation of Optical and Infrared Lines

The ground term of Fe II is the high multiplicity sextet $3d^6 4s^6 D_{\frac{9}{2}, \frac{7}{2}, \frac{5}{2}, \frac{3}{2}, \frac{1}{2}}$. The transitions potentially affected by ultraviolet continuum fluorescence from the ground state should therefore be other sextets of opposite parity, *e.g.* $3d^6 4p^6 (D, F, P)_J^o$, all around 6 eV, resulting in transitions usually labeled $uv1$, $uv2$, $uv3$ respectively. These can influence the low-lying optical and IR transitions via cascades, as shown in Figure 14, but two effects diminish the importance of continuum fluorescence: (1) the number of excited sextet levels is relatively small and the subsequent cascades are via inter-combination transitions (Figure 14), and (2) the source is outside the BLR cloud and photons cannot penetrate to layers where the effective branching ratio favors optical-infrared emission. Therefore ultraviolet pumping from the ground state is not likely to be a dominant mechanism for the enhancement of line emissivities of optical and IR lines among low-lying levels, although individual line ratios may be affected (Bautista & Pradhan 1998). Excitation from the ground a^6D state, at temperatures characteristic of Fe II emitting region of $\approx 10^4$ K, proceeds mainly through electron impact excitation and produces only the low-lying optical-infrared lines shown in Figure 14. Lines originating from higher levels must be excited through other mechanisms, either through ($e^- + \text{ion}$) recombination or fluorescent excitation from low-lying metastable levels which are collisionally populated.

As most of the excited levels of Fe II are of quartet multiplicity, fluorescent excitation is most likely to involve transitions between quartet symmetries originating from low-lying, even parity, metastable levels. For Ly α pumping in particular, the most likely transitions are from the lowest excited quartet state, $3d^6 4s^2 a^4D^e$ to odd parity excited quartet levels (Johansson & Jordan 1984). Table 1, Figure 2, and Figure 15 show such levels accessible within ± 3 Å of Ly α . As shown in SP98, the initial decays from Ly α excitation of a^4D^e results in a group of lines in the $8000 - 9500$ Å range, with a large predicted feature at about 9200 Å. This excitation decay path is explicitly shown in Figure 15.

These sub- μm lines have recently been detected in a supernova remnant, SN 1995N, which is a Type IIn supernova with narrow emission lines originating from circumstellar gas photoionized by X-rays from the shock (Fransson *et al.* 2001). Although the conditions do not quite correspond to the BLRs of AGN, there is still striking agreement between the observed spectra from $8000 - 9500$ Å and the theoretical fits including the Fe II line fluxes computed by the SP98 models. In addition, Fransson *et al.* find that the corresponding Fe II lines, $\lambda\lambda 2506/2508$ Å, indicative of this Ly α pumping path (see Figure 15), are the strongest such features in the UV. We note that in our comparison to the UV spectrum of I Zw 1 (Figure 12) the Fe II feature just redward of Mg II h & k is only reproducible by our models which include Ly α fluorescent

excitation.

$\text{Ly}\alpha$ fluorescence can also involve excitation from several other low-lying, metastable levels (see Figure 2). An important example is excitation from the a^4G^e levels about 3 eV above the ground state. The resultant cascades can form a series of Fe II lines near 1 μm . Figure 15 also depicts this excitation/decay path in quartet multiplet.

These 1 μm lines have been discussed by Rudy *et al.* (2000) in observations of I Zw 1, and by Rodriguez-Ardila *et al.* (2001) in a sample of narrow-line Seyfert galaxies. Rodriguez-Ardila *et al.* also provide the first AGN observations of the primary cascade lines of Fe II near $\lambda 9200 \text{ \AA}$ due to $\text{Ly}\alpha$ pumping. As noted, the excitation-cascade mechanism for the 1 μm lines entails excitation via $a^4G^e \rightarrow (t, u)^4G^o$, followed by downward UV transitions to b^4G^e via $\lambda\lambda 1870/1873$ and $1841/1845 \text{ \AA}$ (see Figure 15). Further transitions within the $b^4G^e - z^4F^o$ multiplet then gives rise to the lines near 1 μm . Rodriguez-Ardila *et al.* also report these lines from narrow-line Seyferts similar to I Zw 1. Earlier, Rudy *et al.* argued against the $\text{Ly}\alpha$ fluorescent mechanism on the grounds that the UV feed lines are not seen in the spectrum of I Zw 1 (see Laor *et al.* 1997), thus suggesting electron collisional excitation as a viable mechanism. In their analysis, however, Rudy *et al.* did not consider one of the UV multiplets, $a^4G^e \rightarrow u^4G^o$, that give rise to the 1841/1845 \AA lines. Our inclusion of both the $(t, u)^4G^o$ levels is based on theoretical calculations of Fe II energy levels and transition probabilities of Nahar (1995). The observations of Rodriguez-Ardila *et al.* (2001) confirm that $\text{Ly}\alpha$ pumping is a strong contributor to the formation of 1 μm lines (suggested in this work and SP98), although collisional excitation, and possibly ($e^- + \text{ion}$) recombination, may be needed to account for the observed intensities (see Figure 11). Discrepancies with observations may also be attributable to uncertainties in our atomic data, particularly the collision strengths.

5. CONCLUSIONS

Multi-level, accelerated lambda-operator techniques for non-LTE radiative transfer now allow solutions to be obtained for highly realistic atomic models including complex cases of line-overlap and fluorescent excitation. Coupled with the new atomic data from the Iron Project, such techniques have been applied for the first time with a reasonably complete Fe II atomic model to theoretical AGN BLR spectra. The theoretical Fe II line fluxes presented should help in the identification of Fe II transitions in AGNs and related sources, and in the delineation of excitation mechanisms producing the Fe II spectrum.

We are extending the calculations to include the line spectra of other iron ionization stages, principally Fe I and Fe III. Laor *et al.* (1997) and Vestergaard & Wilkes (2001) specifically note the present of significant Fe III in the spectrum of I Zw 1, and Graham *et al.* (1996) have detected Fe III emission in the ultra-strong Fe II emitter 2226-3905. Kwan *et al.* (1995) have detected Fe I emission in two Fe II-strong quasars, IRAS 07598+6508 and PHL 1092. Simultaneous modeling of these ionization stages should provide more constraints on the nature of the iron emission.

Our calculations currently include transitions between observed energy levels whereas there remains a large number of theoretically predicted energy levels. We are in-

cluding these levels and the implied radiative transitions in order to provide a much more complete description of the Fe II emission spectrum.

We are currently working on bringing the entire photoionization calculation for all atoms and ions within the framework of exact radiative transfer established in this work. This will allow a self-consistent treatment of the Fe II emission by including it in the net heating/cooling which determines the temperature structure, and will also allow an *exact* treatment of $\text{Ly}\alpha$ fluorescent excitation of Fe II emission.

We are also working on several other specific problems, such as the interpretation of Fe II/Mg II line ratios, employing extended non-LTE models for the relevant atomic species and exact radiative transfer.

The tabular and graphical material presented in this work is available electronically on request.

We would like to thank Sultana Nahar for numerous contributions, and Marianne Vestergaard for the data in Figure 12. This work was supported by the Natural Sciences and Engineering Research Council of Canada (TAAS), and by the U.S. National Science Foundation and NASA (AKP).

REFERENCES

Aoki, K., Murayama, T., & Denda, K. 2002 PASP submitted (astro-ph/0204505)

Avrett, E. H., & Loeser, R. 1988 ApJ 331, 211

Baldwin, J., Ferland, G., Korista, K., & Verner, D. 1995 ApJ 455, L119

Basri, G.S. 1980 ApJ 242, 1133

Bautista, M. A., & Pradhan, A. K. 1995 A&A S 115, 551

Boroson, T.A., & Green, R.F. 1992 ApJS 80, 109

Burke, P. G., & Berrington, K. A. 1993 *Atomic and Molecular Process: An R-matrix Approach* (Institute of Physics Publishing : Bristol)

Collin-Souffrin, S., Dumont, S., Heidman, N., & Joly, M. 1980 A&A 83, 190

Corbin, M., & Boroson, T.A. 1996 ApJS 107, 69

Dietrich, M., Appenzeller, I., Vestergaard, M., & Wagner, S.J. 2002 ApJ 564, 581

Elitzur, M., & Netzer, H. 1985 ApJ 291, 464

Elston, R., Thompson, K.L., & Hill, G.J. 1994 *Nature* 367, 250

Ferland, G. 1991, HAZY: An Introduction to CLOUDY, OSU Internal Report, 91-01

Flower, D. 1990 *Molecular Collisions in the Interstellar Medium* (Cambridge University Press: Cambridge)

Fransson, C., Chevalier, R.A., Filippenko, A.V., Leibundgut, B., Barth, A.J., Fesen, R.A., Kirshner, R.P., Leonard, D.C., Li, W., Lundqvist, P., Sollerman, J., & Van Dyk, S.D. 2001 ApJ (submitted, astro-ph/0108149)

Fuhr, J.R., Martin, G.A., & Wiese, W.L. 1988, J. Phys. Chem. Ref. Data, 17, 1

Graham, M. J., Clowes, R. G., & Campusano, L. E. 1996 MNRAS 279, 1349

Grandi, S. A. 1981 ApJ 251, 451

Hamann, F., & Ferland, G. 1992

Hamann, F., & Ferland, G. 1999 ARA&A 37, 487

Hummer, D. G., & Mihalas, D. 1967 ApJ 150, L57

Hummer, D. G., Berrington, K. A., Eissner, W., Pradhan, A. K., Saraph, H. E., & Tully, J. A. 1993 A&A 279, 298

Iwamuro, F., Motohara, K., Maihara, T., Kimura, M., Yoshii, Y., & Doi, M. 2002 ApJ565, 63

Johansson, S. 1978 Phys. Scr. 18, 217

Johansson, S., Jordan, C. 1984 MNRAS 210, 239

Joly, M. 1987, A&A184, 33

Joly, M. 1993 Ann. Phys. Fr. 18, 241

Kingdon, J. B., & Ferland, G. J. 1996 ApJS 106, 205

Kneer, F. ApJ 200, 367

Kwan, J., Cheng, F-Z., Fang, L-Z., Zheng, W., & Ge J. 1995, ApJ 440, 628

Kurucz, R.L. 1981, Semi-Empirical Calculation of gf-Values: Fe II, SAO Rep. 390 (Cambridge: SAO)

Laor, A., Jannuzzi, B.T., Green, R.F., & Boroson, T.A. 1997 ApJ 489, 656

Lipari, Macchett, F., & Golombek, D. 1991 ApJ 366, L65

Mathews, W.G., & Ferland, G.J. 1987 ApJ 323, 456

Marziani, P., Sulentic, J.W., Dultzin-Hacyan, D., Calvani, M., & Moles., M. 1996, ApJS 104, 37

Mihalas, D. 1978 *Stellar Atmospheres*, 2nd edition (W. H. Freeman & Company : San Fransico)

Nahar, S. N. 1995 A&A 293, 967

Nahar, S. N. 1996 Phys. Rev. A 53, 1545

Nahar, S. N., & Bautista 1999 ApJS 120, 327

Nahar, S. N., 1997 Phys. Rev. A 55, 1980

Netzer, H. 1980 ApJ 236, 406

Netzer, H., & Wills, B. J. 1983 ApJ 275, 445

Netzer, H. 1988 in *Physics of Formation of Fe II Lines Outside of LTE*, R. Viotti, A. Vittone & M. Friedjung (eds) (D. Reidel Publishing Company: Dordrecht), p. 247

Neufeld, D. A., & Dalgarno, A. 1987 Phys. Rev. A 35, 3142

Osterbrock, D. E., & Pogge 1985, ApJ 297, 166

Penston, M. V. 1987 MNRAS 229, 1p

Rodriguez-Ardila, A., Viegas, S.M., Pastoriza, M.G., & Prato, L. 2001 ApJ (in press, astro-ph/0109516)

Rudy, R.J., Mazuk, S., Puetter, R.C., & Hamann,F. 2000 ApJ 539, 166

Rybicki, G. B., & Hummer, D. G. 1991 A&A 245, 171

Rybicki, G. B., & Hummer, D. G. 1992 A&A 262, 209

Sigut, T.A.A. & Pradhan, A.K. 1998, ApJ 499, L139 (SP98)

Thompson, Hill, & Elston 1999

Vestergaard, M. & Wilkes, B.J. 2001, ApJS 134, 1

Viotti, R. 1988 in *Physics of Formation of Fe II Lines Outside of LTE*, R. Viotti, A. Vittone & M. Friedjung (eds) (D. Reidel Publishing Company: Dordrecht), p. 331

Wills, B. J., Netzer, H., Uomoto, A. K., & Wills, D. 1980 ApJ 237, 319

Wills, B. J., Netzer, H., & Wills, D. 1985 ApJ 288, 94

Vernazza, J. E., Avrett, E. H., & Loeser, R. 1981 ApJS 45, 635

Verner, E.M., Verner, D.A., Korista, J.W., Ferguson, J.W., Hamann, F., & Ferland, G.J. 1999 ApJS 120, 101

Zamanov, R., & Marziani, P. 2002 ApJ submitted (astro-ph/0204423)

Zhang, H. L., & Pradhan, A. K. 1995 A&A 293, 9531

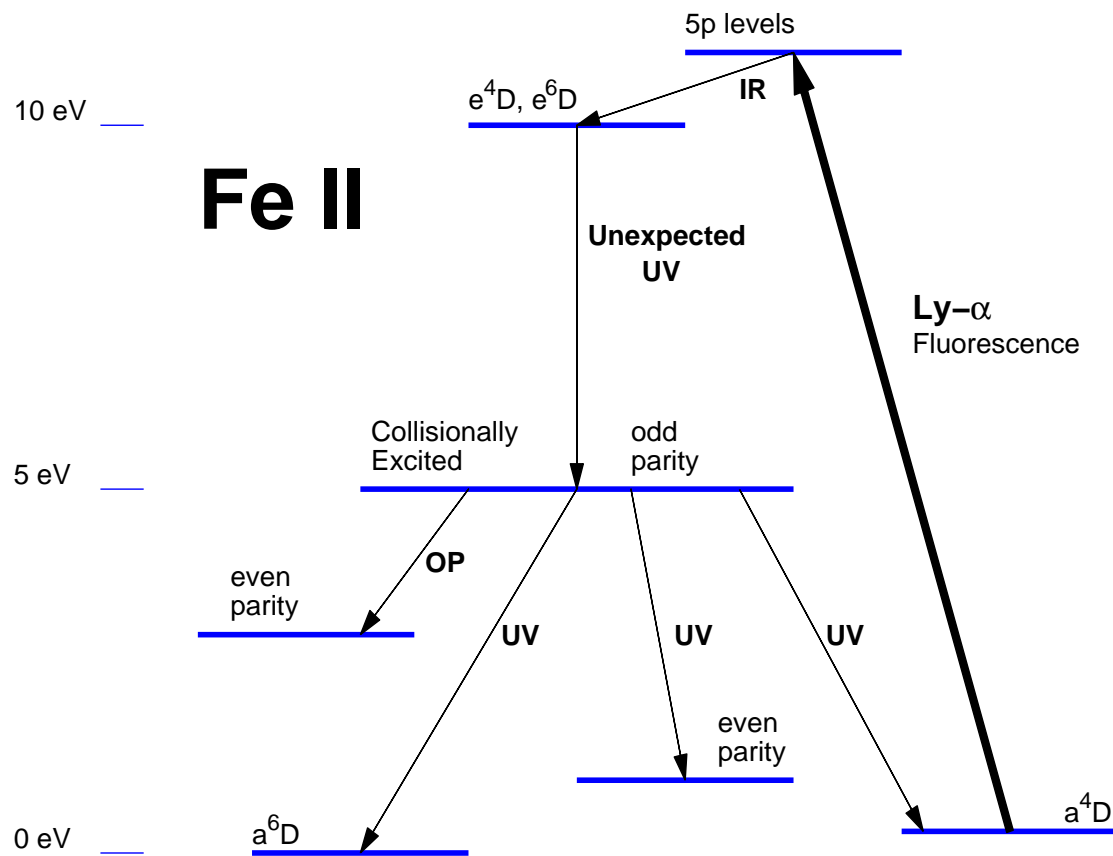


FIG. 1.— A highly simplified Fe II Grotian diagram illustrating the main excitation mechanisms discussed in the text.

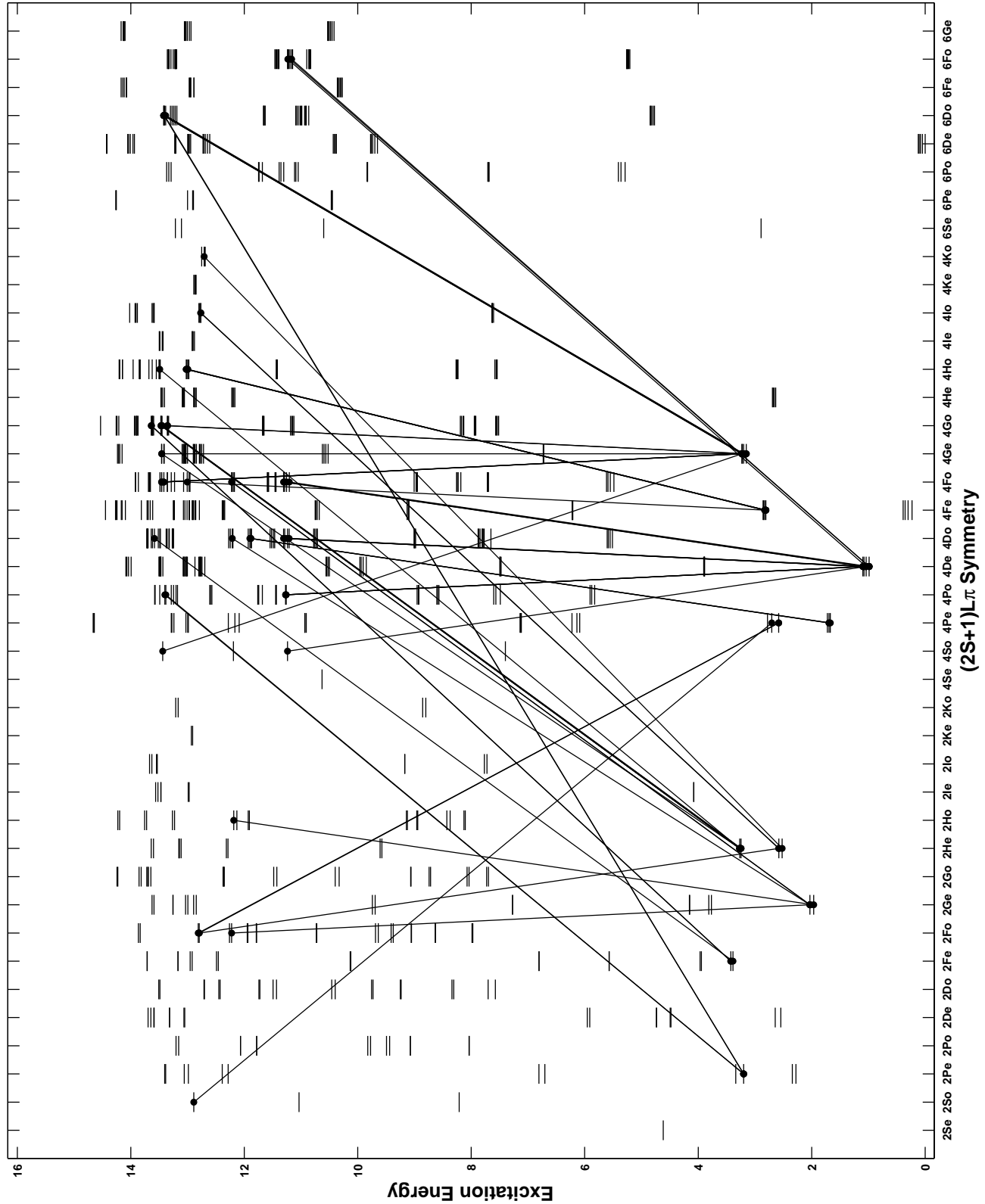


FIG. 2.—An Grotrian diagram showing all 827 Fe II energy levels (with the exception of a few levels in the octet spin system). Solid lines connect transitions within $\pm 3 \text{ \AA}$ of Ly α and represents only a small fraction of the 23,000 radiative transitions included in the calculations.

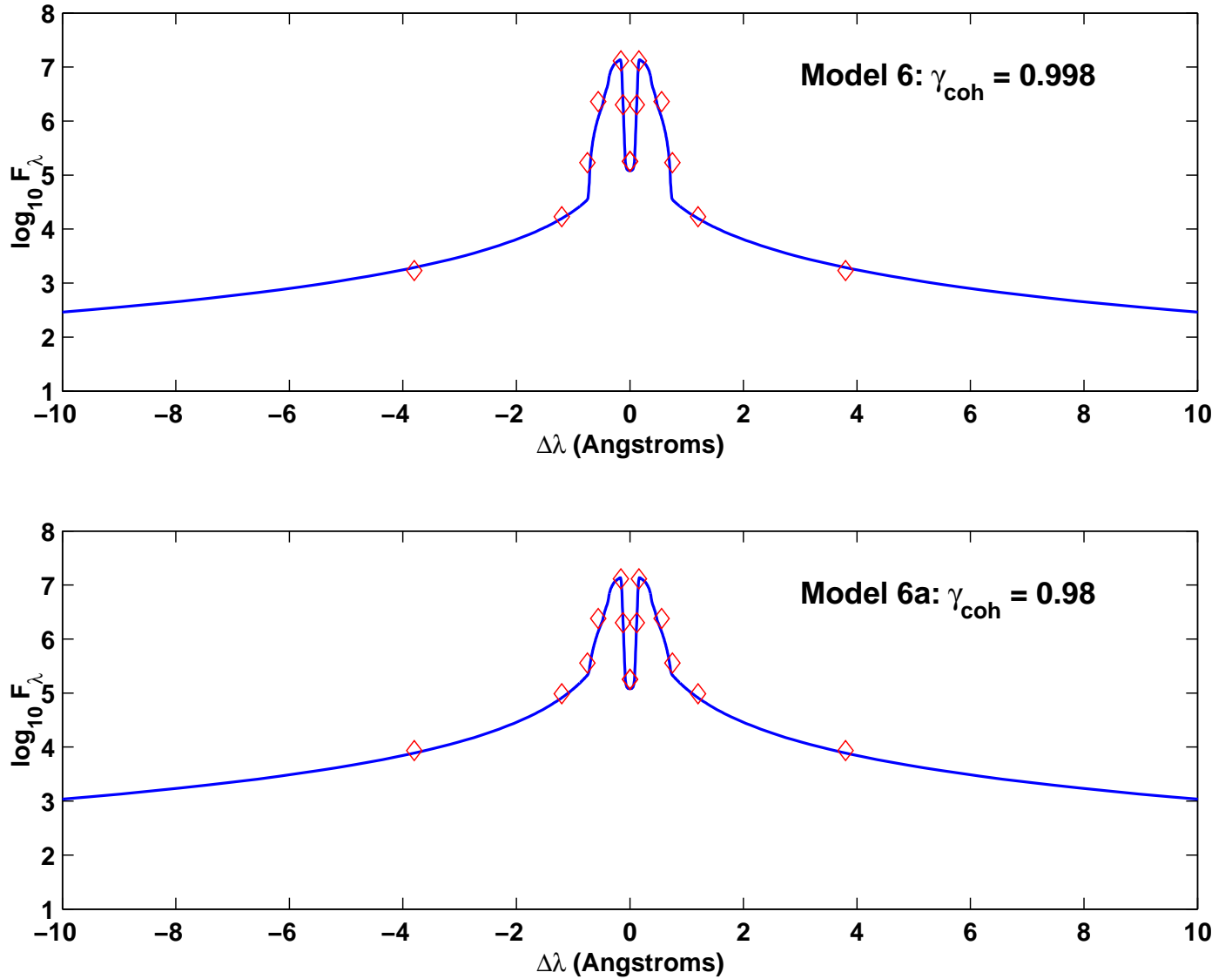


FIG. 3.— Comparison between the Ly α profiles of Avrett & Loeser (1988, diamonds) with those calculated in the current work using the same BLR model (solid lines). The fraction of coherently scattered Ly α photons, γ_{coh} , is indicated in each panel.

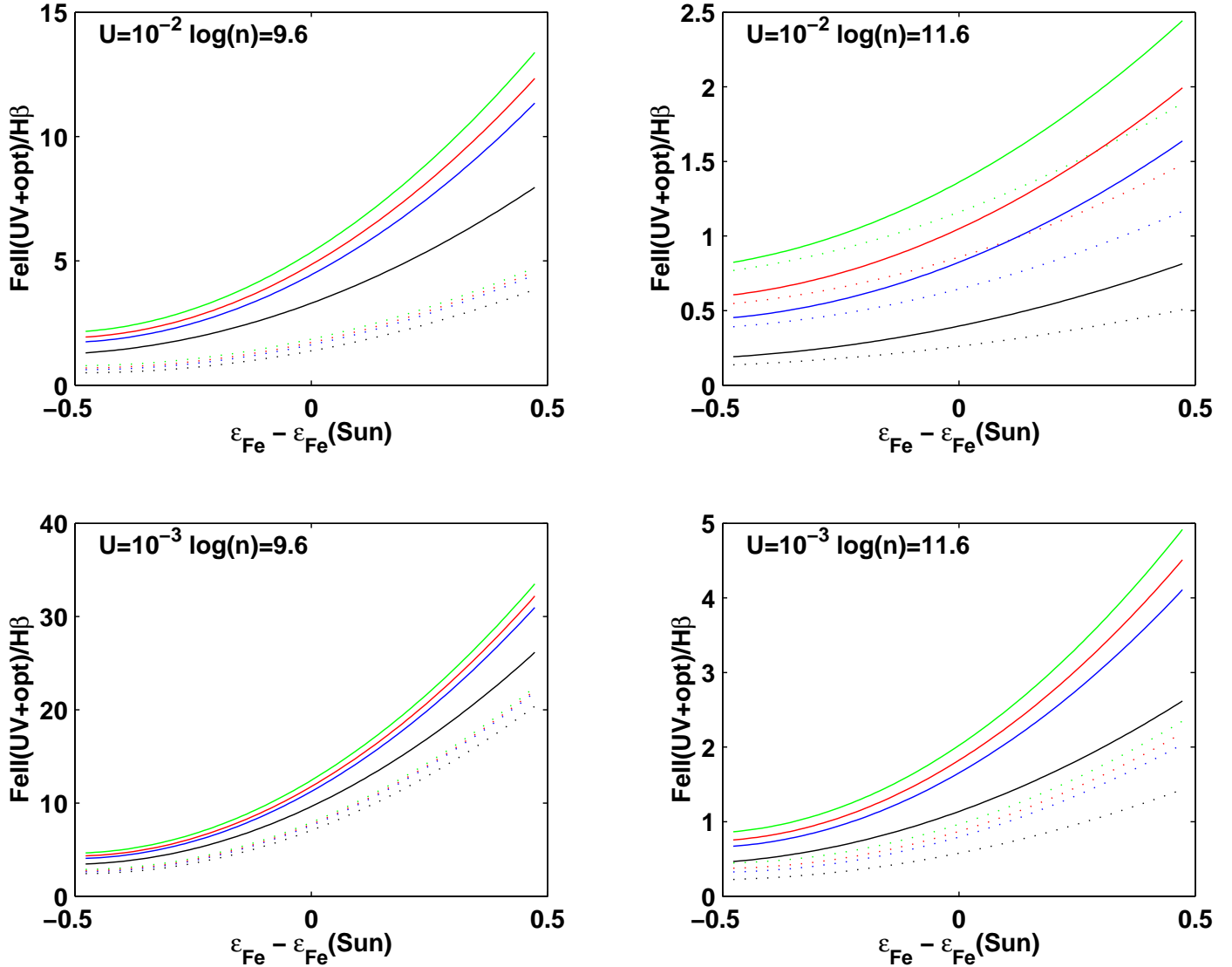


FIG. 4.— The dependence of the total predicted Fe II UV+Opt flux on the iron abundance (ϵ_{Fe}) and internal cloud microturbulent velocity (ζ_t). Each panel represents one of the BLR cloud models of Table 2. Two calculations are presented for each model, one including fluorescent excitation (both Ly α and Ly β , solid lines) and one not including fluorescent excitation (dotted lines). At each abundance, the lines in order of increasing flux correspond to increasing turbulent velocities 0, 10, 20, and 40 km s^{-1} .

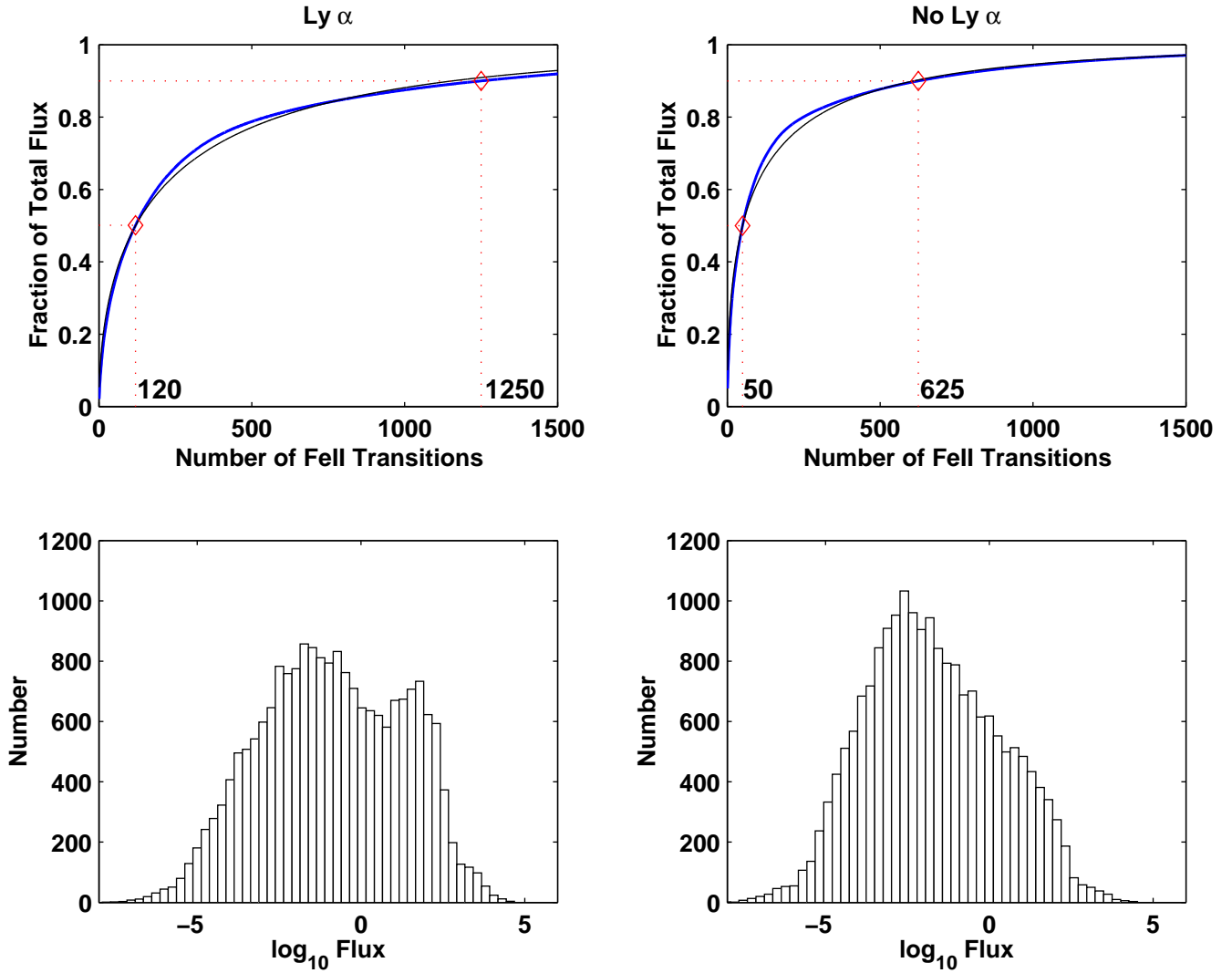


FIG. 5.— The top two panels show the cumulative sum of the Fe II flux with (left) and without (right) Ly α fluorescent excitation. The number of transitions required in the sum to reach 50% and 90% of the total flux are as indicated. The bottom two panels show the distribution of $\log_{10} F$ with (left) and without (right) Ly α fluorescent excitation. BLR model A was used for all calculations.

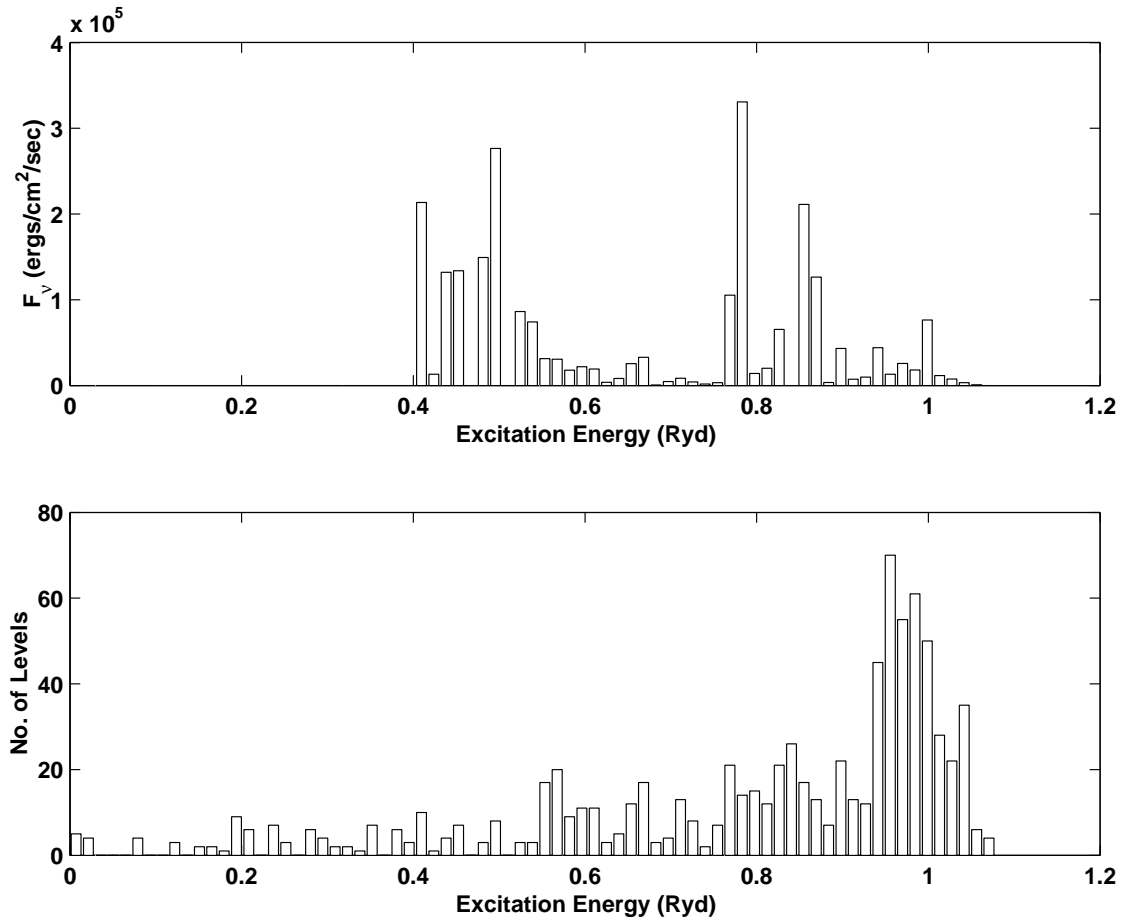


FIG. 6.— The lower panel shows a histogram of the number of included Fe II levels within each energy bin. The upper panel shows the total flux arising from transitions with upper levels in each bin for BLR model A including fluorescent excitation.

FIG. 7.—The predicted flux and line identifications for 1600–2300 Å for BLR model A with Ly α and Ly β fluorescence.

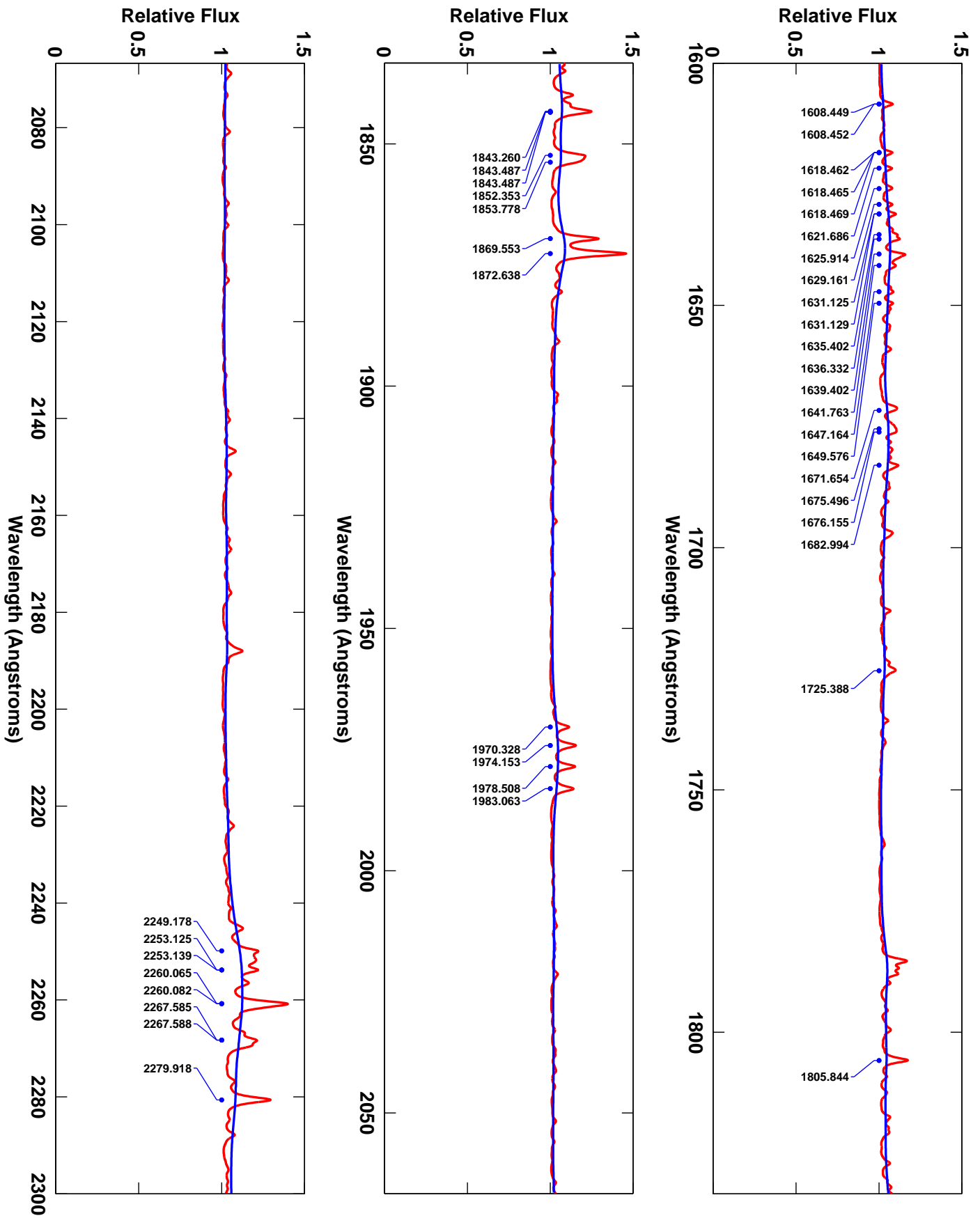


FIG. 8.—The 2300-2700 Å region predicted for AGN model A with Ly α and Ly β fluorescence.

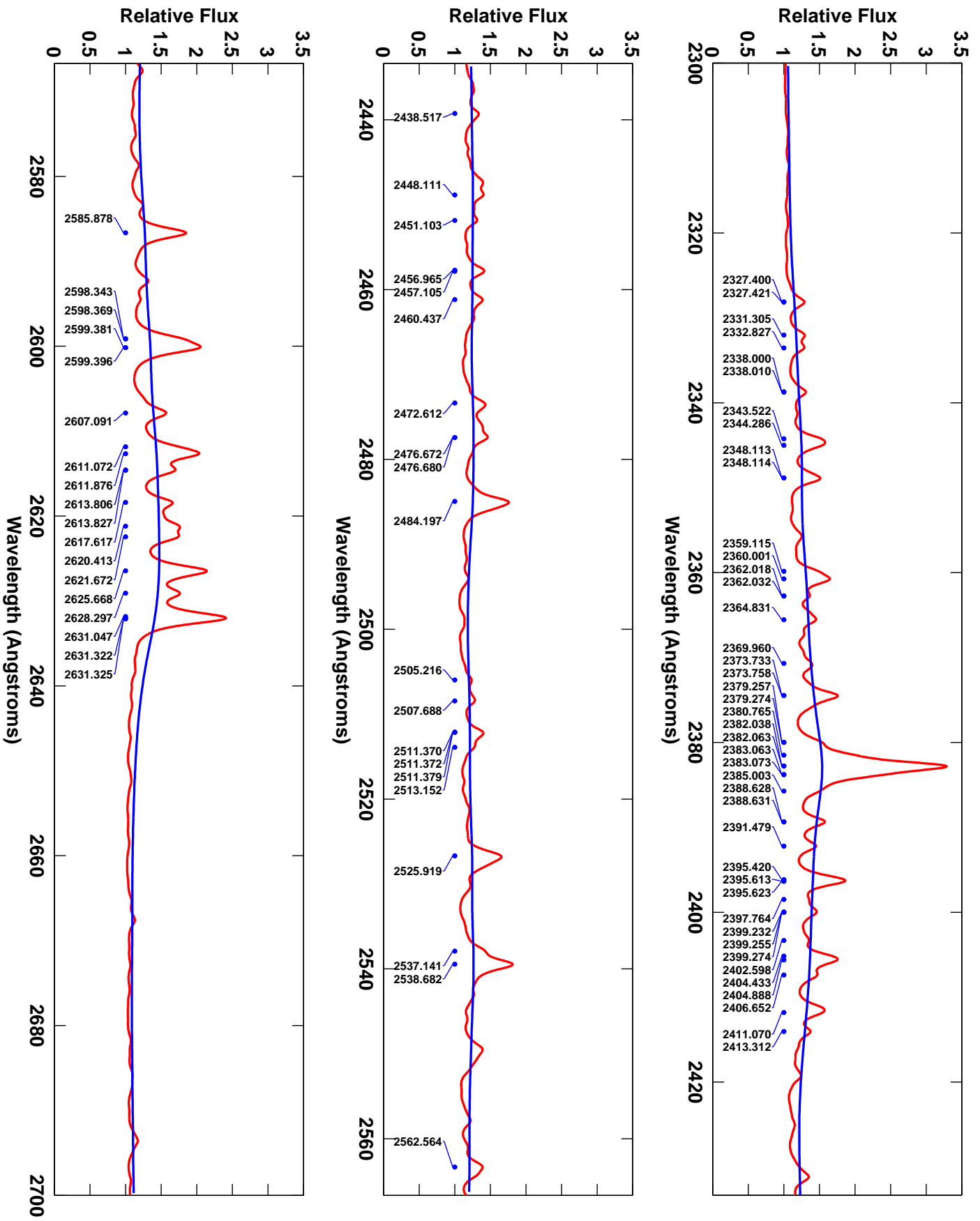


FIG. 9.—The 2700–3100 Å region predicted for AGN model A with Ly α and Ly β fluorescence.

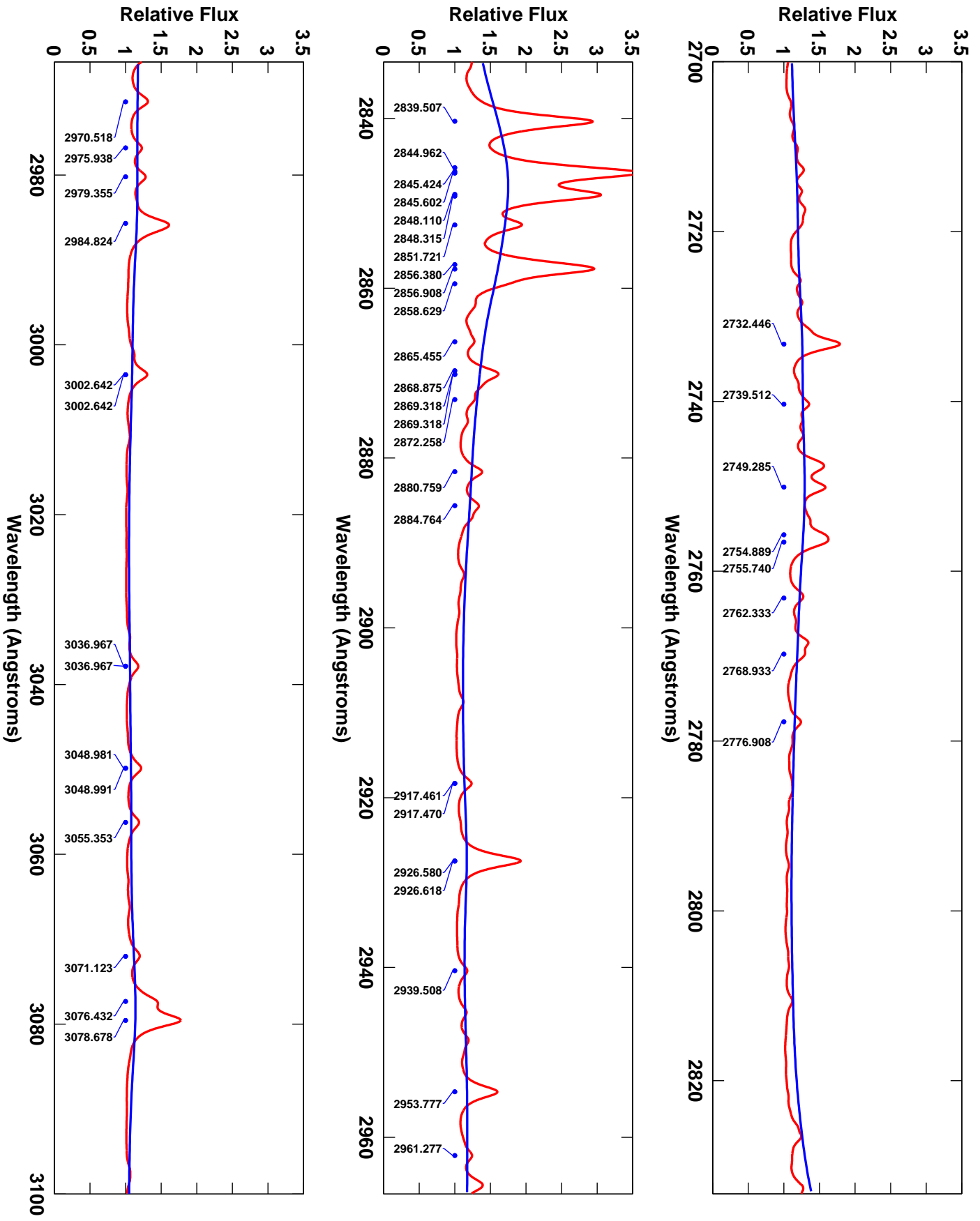


FIG. 10.—The 3100–7000 Å region predicted for AGN model A with Ly α and Ly g fluorescence.

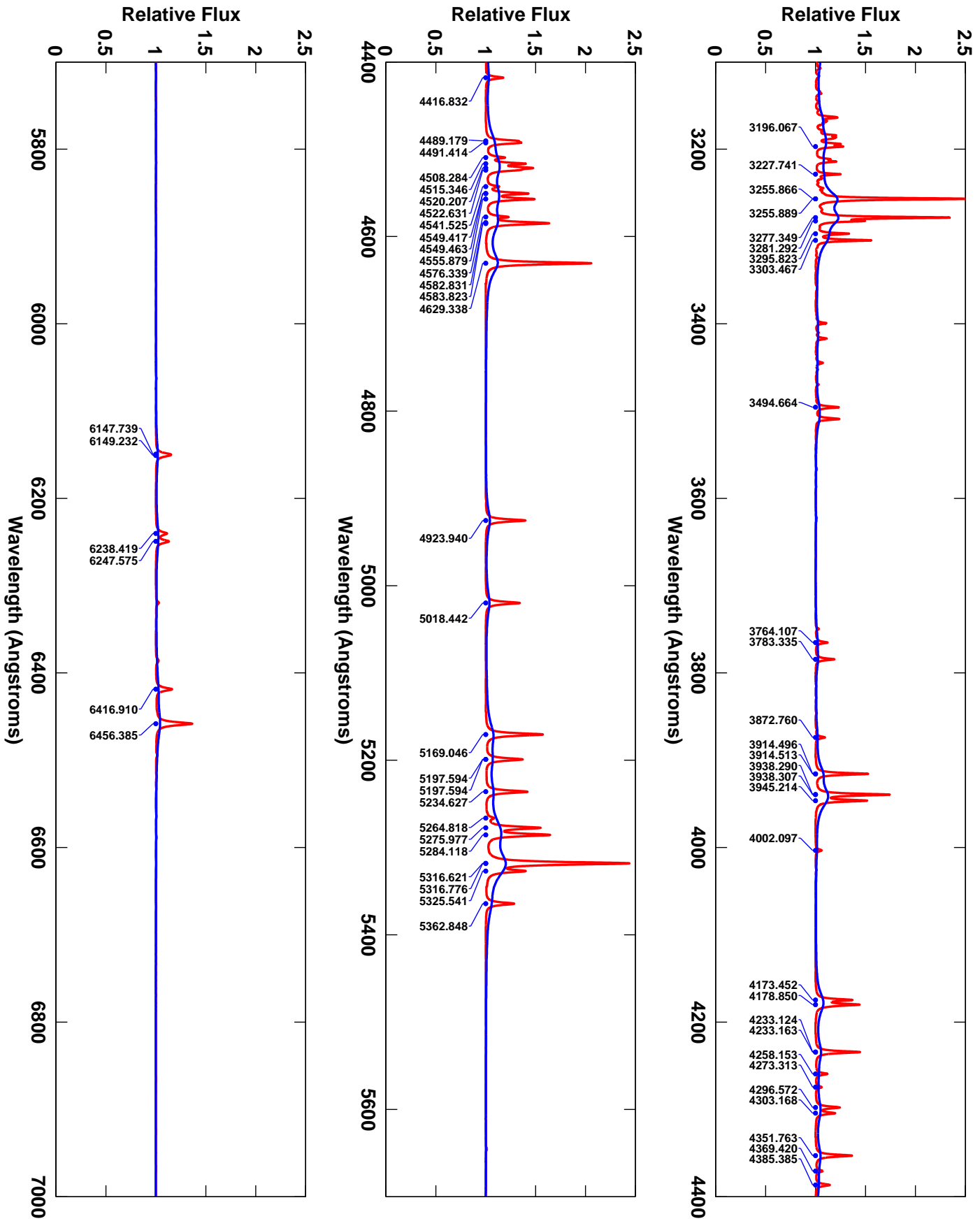
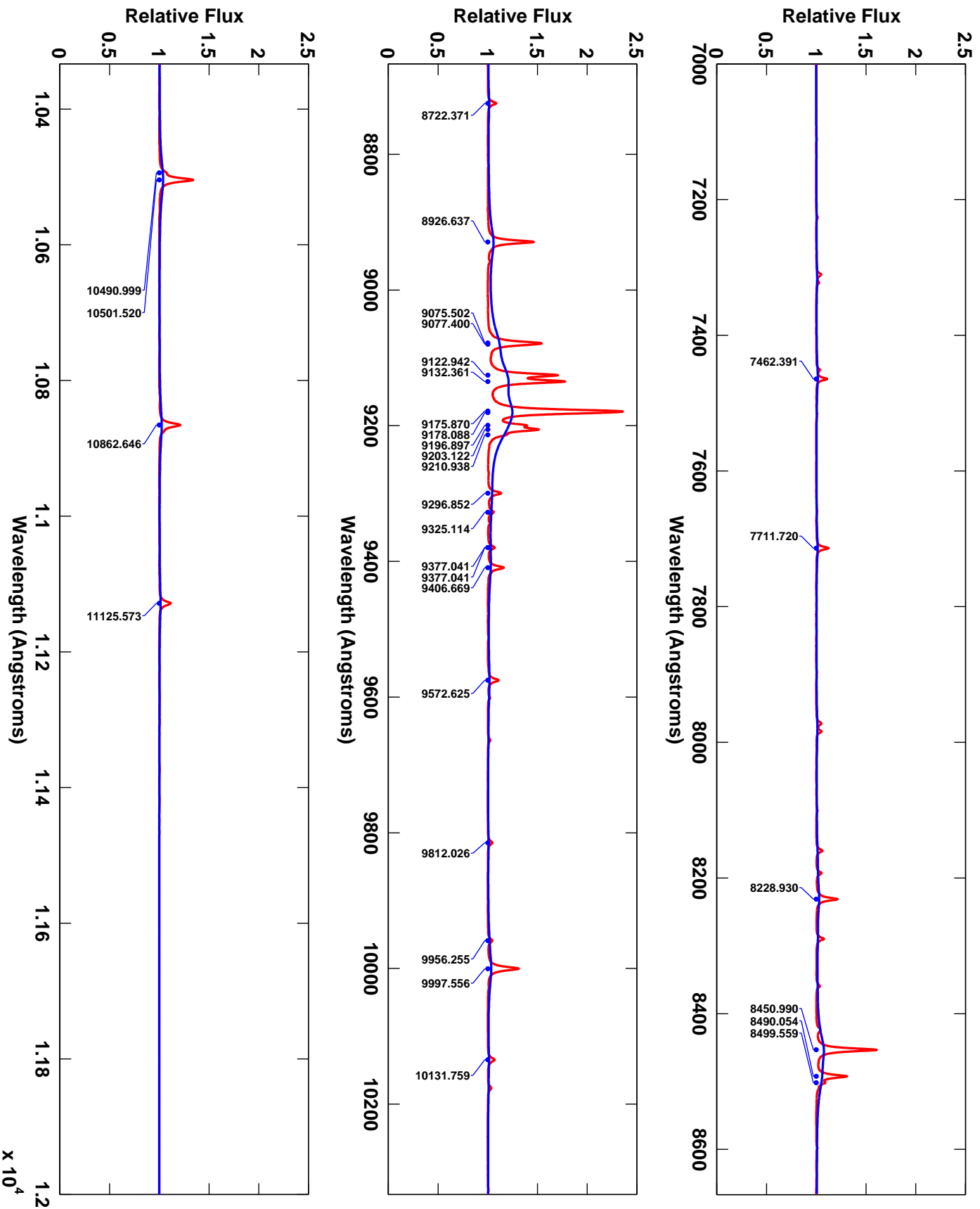


FIG. 11.—The 7000-1200 Å region predicted for AGN model A with Ly α and Ly β fluorescence.



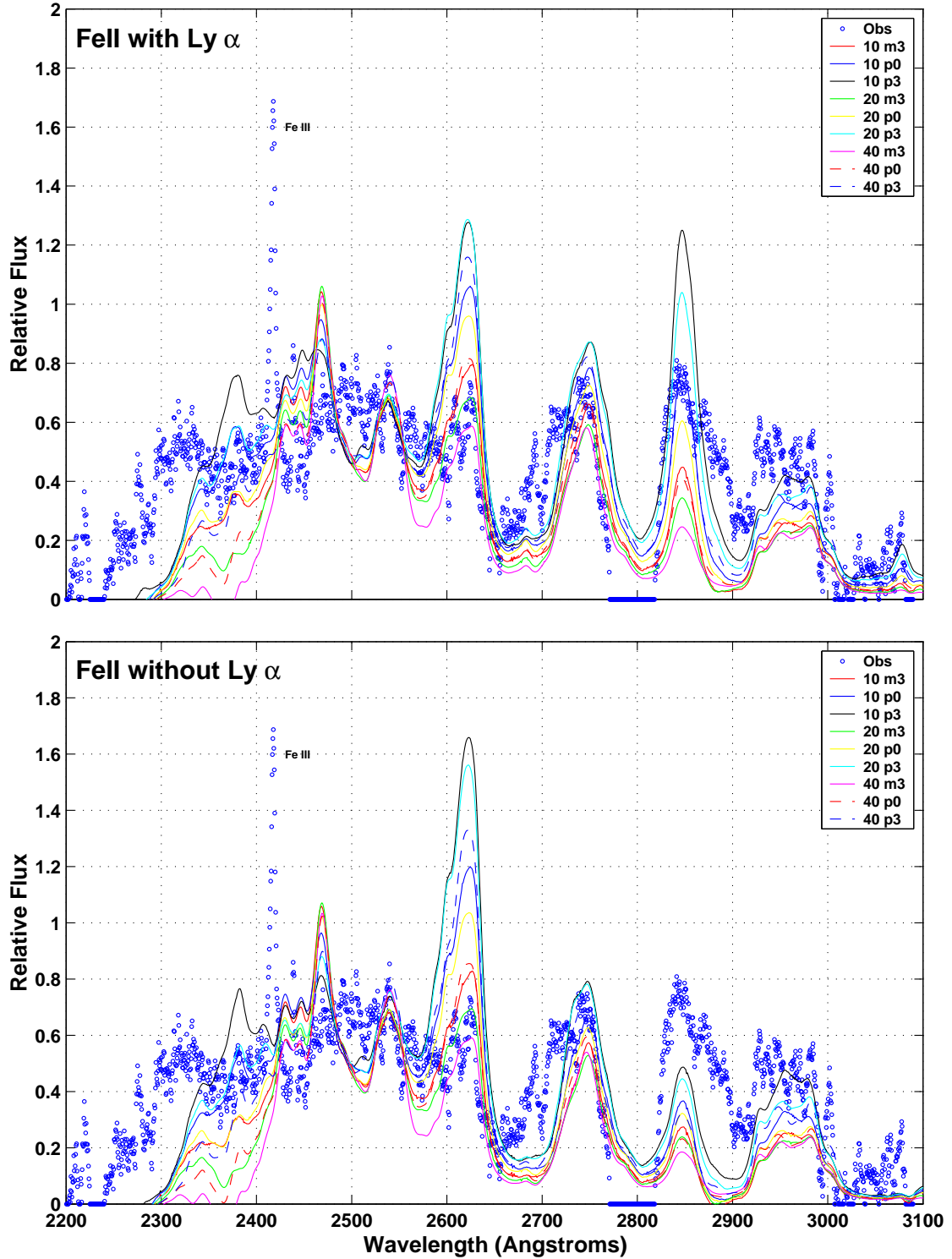


FIG. 12.— A comparison of the predicted UV Fe II spectrum corresponding to model B of Table 2 and the empirical UV Fe II - Fe III template of Vestergaard & Wilkes (2001). The upper panel includes fluorescent excitation while the lower panel does not. The various colours and line styles correspond to different combinations of iron abundance and cloud turbulence velocity as indicated by the legend in each panel.

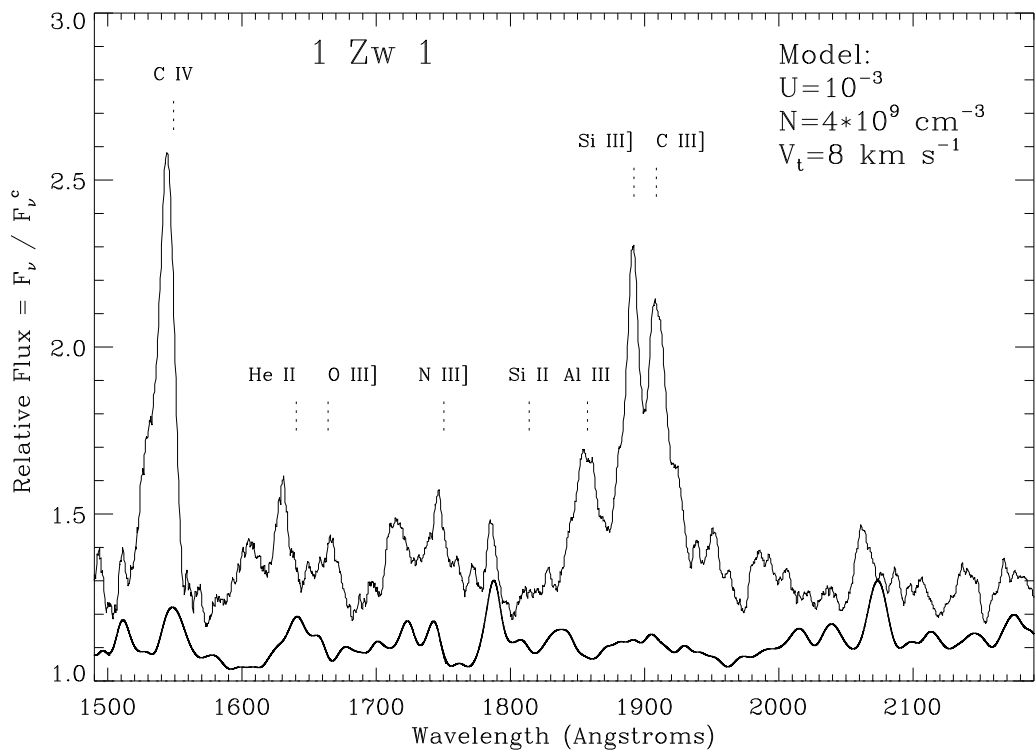


FIG. 13.— The UV spectrum of I Zw 1 (Marziani *et al.* 1996) compared to the theoretical Fe II spectra. The observed spectrum has been smoothed over 15 pixels and rectified to a power-law continuum ($F^c = 11(1500\text{\AA}/\lambda)^{1.1}$). The observations are off-set by +0.1 for clarity. A few of the prominent emission lines in this region are identified using Table 4A of Laor *et al.* (1994).

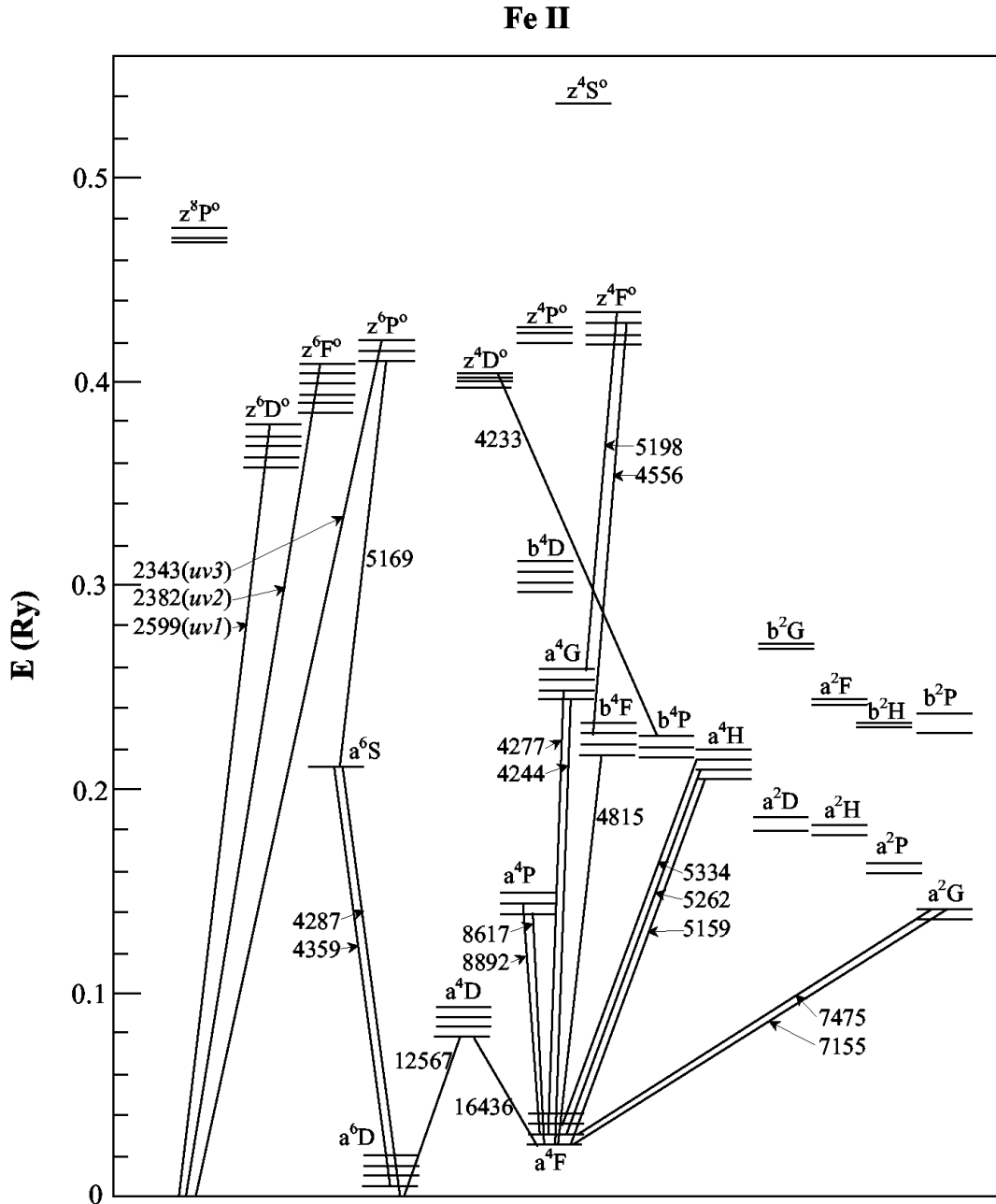


FIG. 14.— A partial Grotrian diagram for Fe II showing the low-lying optical and infrared transitions.

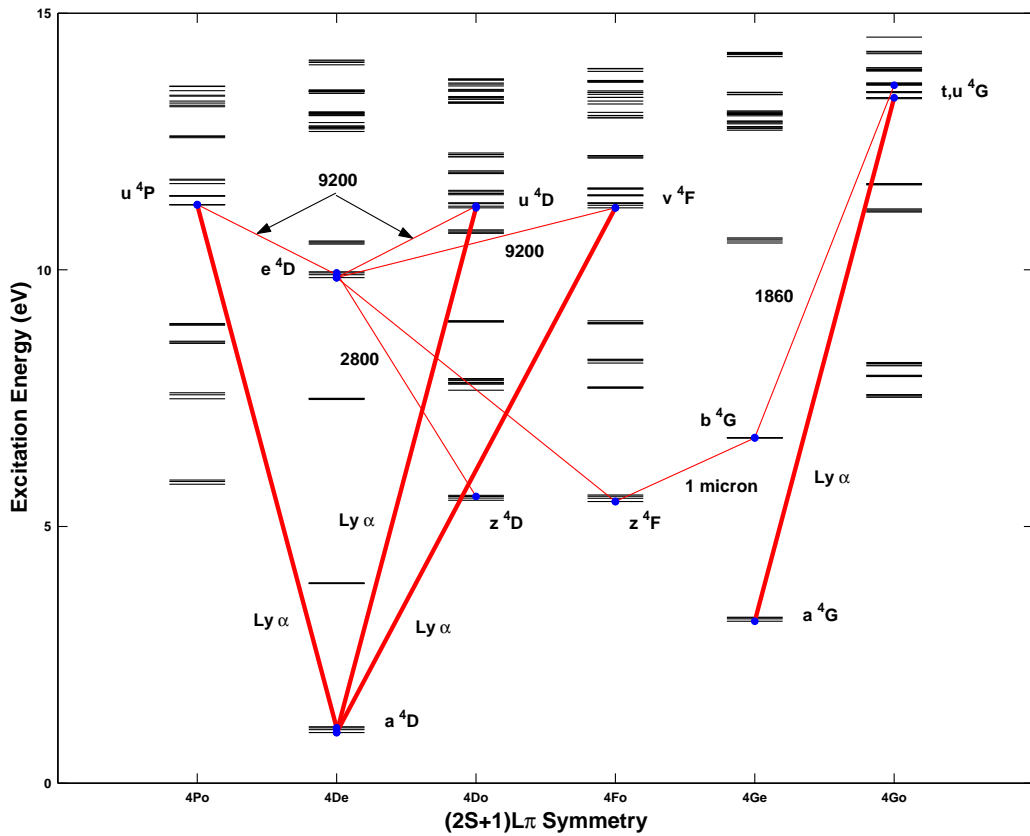


FIG. 15.— The 1 μ m IR lines and the $\lambda 9220 \text{ \AA}$ features in the Fe II quartet system, showing the Ly α fluorescence and cascade routes. The 1 μ m lines correspond to multiplet transitions $b^4G - z(^4F^o, ^4D^o)$ given at the end of Table 11; see the text for details.

TABLE 1
FE II TRANSITIONS FROM a⁴D^e WITHIN $\pm 3\text{\AA}$ OF Ly α .

λ (\AA)	$\Delta\lambda/\Delta\lambda_D$	Transition $l \rightarrow u$	log(gf)		
			N96	K91	K81
1212.97	-51.9	a ⁴ D _{7/2} ^e - u ⁴ D _{7/2} ^o	-1.78	-1.47	-2.39
1213.13	-48.7	a ⁴ D _{7/2} ^e - v ⁴ F _{9/2} ^o	-0.72	-1.18	-1.70
1213.74	-37.1	a ⁴ D _{3/2} ^e - u ⁴ F _{5/2} ^o	-1.07	-1.31	-2.16
1213.76	-36.7	a ⁴ D _{5/2} ^e - u ⁴ F _{7/2} ^o	-0.89	-1.17	-1.95
1214.07	-30.8	a ⁴ D _{3/2} ^e - u ⁴ D _{3/2} ^o	-2.42	-1.73	-3.67
1214.15	-29.2	a ⁴ D _{1/2} ^e - v ⁴ F _{3/2} ^o	-1.28	-1.49	-2.39
1214.29	-26.6	a ⁴ D _{1/2} ^e - u ⁴ D _{1/2} ^o	-2.63	-2.16	-3.25
1214.40	-24.4	a ⁴ D _{7/2} ^e - x ⁶ F _{7/2} ^o	-2.23	-2.40	
1215.85	+3.5	a ⁴ D _{5/2} ^e - u ⁴ D _{5/2} ^o	-2.09	-2.03	-2.55
1215.98	+6.0	a ⁴ D _{5/2} ^e - y ⁴ S _{3/2} ^o	-3.05	-4.63	
1216.27	+11.6	a ⁴ D _{3/2} ^e - u ⁴ P _{3/2} ^o	-1.42	-2.35	-2.97
1216.52	+16.4	a ⁴ D _{1/2} ^e - u ⁴ D _{3/2} ^o	-2.63	-2.31	-2.36
1217.15	+28.5	a ⁴ D _{3/2} ^e - u ⁴ P _{1/2} ^o	-1.52	-2.22	-4.55
1217.85	+41.8	a ⁴ D _{7/2} ^e - x ⁶ F _{9/2} ^o	-1.49	-2.27	
1218.09	+46.4	a ⁴ D _{5/2} ^e - u ⁶ F _{5/2} ^o	-3.10	-2.78	
⟨shift⟩ relative to N96			+0.09	-1.04	
σ relative to N96			+0.51	+0.82	

Note. — $\Delta\lambda_D$ is the Doppler width of Ly α at 10^4 K. The references for the log(gf) are N96 (Nahar 1996), K91 (Kurucz 1991), and K81 (Kurucz 1981). The shift and σ entries refer to the average differences and standard deviations relative to N96. This list is only the closest lines in the models including Ly α pumping.

TABLE 2
THE FOUR AGN CLOUD MODELS CONSIDERED IN THIS WORK.

Model	U_{ion}	$\log_{10} N_H$	$\log_{10} F_{H\beta}$
A	10^{-2}	9.6	5.68
B	10^{-2}	11.6	7.20
C	10^{-3}	9.6	4.55
D	10^{-3}	11.6	6.70

Note. — The shape of the photoionizing continuum was taken from Mathews & Ferland (1988).

TABLE 3
FE II FLUXES FOR THE MODEL A WITH Ly α AND Ly β PUMPING.

$\lambda(\text{\AA})$	Upper	Lower	$E_l(\text{eV})$	Flux	$\lambda(\text{\AA})$	Upper	Lower	$E_l(\text{eV})$	Flux
927.174	$u^6D_{7/2}^o$	$a^6D_{7/2}^e$	0.048	9.89^{+2}	1309.555	$x^2I_{11/2}^o$	$a^2I_{11/2}^e$	4.079	7.38^{+2}
1133.674	$u^4D_{5/2}^o$	$a^4F_{7/2}^e$	0.301	5.59^{+3}	1310.589	$t^2H_{11/2}^o$	$b^2G_{9/2}^e$	3.766	7.31^{+2}
1135.578	$u^4P_{3/2}^o$	$a^4F_{5/2}^e$	0.352	5.18^{+2}	1311.062	$x^2I_{13/2}^o$	$a^2I_{13/2}^e$	4.074	7.30^{+2}
1138.940	$u^4D_{5/2}^o$	$a^4F_{5/2}^e$	0.352	2.43^{+3}	1311.615	$t^2H_{9/2}^o$	$b^2G_{7/2}^e$	3.813	5.48^{+2}
1144.049	$u^6D_{7/2}^o$	$b^4P_{5/2}^e$	2.582	2.28^{+3}	1312.490	$u^4G_{9/2}^o$	$b^4D_{7/2}^e$	3.902	1.33^{+3}
1159.503	$u^4G_{9/2}^o$	$a^4H_{11/2}^e$	2.656	6.04^{+2}	1332.731	$v^6F_{3/2}^o$	$b^4D_{3/2}^e$	3.887	6.42^{+2}
1170.562	$u^6D_{7/2}^o$	$b^4F_{7/2}^e$	2.827	1.15^{+3}	1352.735	$r^4F_{9/2}^o$	$b^4D_{7/2}^e$	3.902	1.20^{+3}
1175.957	$u^4C_{9/2}^o$	$b^4F_{9/2}^e$	2.805	2.89^{+3}	1354.748	$t^2H_{11/2}^o$	$a^2I_{13/2}^e$	4.074	6.39^{+2}
1199.670	$w^4H_{9/2}^o$	$a^4H_{9/2}^e$	2.675	5.69^{+2}	1364.434	$s^2D_{3/2}^o$	$b^2P_{1/2}^e$	3.338	5.96^{+2}
1209.430	$u^4D_{5/2}^o$	$a^4D_{7/2}^e$	0.986	4.18^{+3}	1378.437	$r^2F_{7/2}^o$	$b^2H_{9/2}^e$	3.266	5.05^{+2}
1211.986	$v^4P_{5/2}^o$	$a^4D_{5/2}^e$	1.040	8.10^{+2}	1379.713	$u^4P_{1/2}^o$	$a^2P_{3/2}^e$	2.275	5.46^{+2}
1213.090	$u^6D_{7/2}^o$	$a^4G_{9/2}^e$	3.198	9.28^{+2}	1384.671	$w^6D_{1/2}^o$	$b^4P_{3/2}^e$	2.703	5.18^{+2}
1263.702	$w^4H_{9/2}^o$	$a^4G_{9/2}^e$	3.198	8.34^{+2}	1409.260	$r^2F_{5/2}^o$	$a^2F_{5/2}^e$	3.423	2.58^{+3}
1265.071	$w^4H_{7/2}^o$	$a^4G_{7/2}^e$	3.220	6.41^{+2}	1423.690	$v^4F_{5/2}^o$	$b^4P_{5/2}^e$	2.582	7.84^{+2}
1265.638	$w^4H_{11/2}^o$	$a^4G_{9/2}^e$	3.198	6.38^{+2}	1427.133	$v^4P_{5/2}^o$	$b^4P_{5/2}^e$	2.582	9.68^{+2}
1266.254	$w^4H_{7/2}^o$	$a^4G_{5/2}^e$	3.229	1.18^{+3}	1437.457	$u^4D_{7/2}^o$	$b^4P_{5/2}^e$	2.582	1.63^{+3}
1266.525	$w^4H_{9/2}^o$	$a^4G_{7/2}^e$	3.220	1.55^{+3}	1440.987	$v^4F_{3/2}^o$	$b^4P_{3/2}^e$	2.703	5.13^{+2}
1274.469	$w^4H_{11/2}^o$	$b^2H_{9/2}^e$	3.266	5.03^{+2}	1443.738	$t^2G_{9/2}^o$	$b^2G_{9/2}^e$	3.766	5.35^{+2}
1286.430	$v^4F_{3/2}^o$	$a^4P_{5/2}^e$	1.670	7.92^{+2}	1452.922	$u^4D_{5/2}^o$	$b^4P_{3/2}^e$	2.703	1.56^{+3}
1288.724	$v^4F_{5/2}^o$	$a^4P_{5/2}^e$	1.670	5.28^{+2}	1453.703	$u^4D_{1/2}^o$	$b^4P_{1/2}^e$	2.777	5.16^{+2}
1289.094	$u^4D_{3/2}^o$	$a^4P_{5/2}^e$	1.670	1.13^{+3}	1460.090	$u^4P_{3/2}^o$	$b^4P_{1/2}^e$	2.777	6.26^{+2}
1291.544	$v^4P_{5/2}^o$	$a^4P_{5/2}^e$	1.670	6.84^{+2}	1464.782	$v^4F_{3/2}^o$	$b^4F_{5/2}^e$	2.843	1.57^{+3}
1291.583	$u^4P_{3/2}^o$	$a^4P_{5/2}^e$	1.670	1.07^{+3}	1464.982	$v^4F_{5/2}^o$	$b^4F_{7/2}^e$	2.827	1.90^{+3}
1292.405	$u^4D_{3/2}^o$	$a^4P_{3/2}^e$	1.695	9.22^{+2}	1466.956	$u^4D_{1/2}^o$	$b^4F_{3/2}^e$	2.854	5.48^{+2}
1293.592	$v^4F_{3/2}^o$	$a^4P_{1/2}^e$	1.723	1.16^{+3}	1467.492	$v^4F_{7/2}^o$	$b^4F_{9/2}^e$	2.805	1.64^{+3}
1293.746	$u^4D_{1/2}^o$	$a^4P_{1/2}^e$	1.723	5.26^{+2}	1474.306	$u^4D_{5/2}^o$	$b^4F_{7/2}^e$	2.827	8.26^{+2}
1294.906	$u^4P_{3/2}^o$	$a^4P_{3/2}^e$	1.695	1.12^{+3}	1474.597	$r^2F_{5/2}^o$	$b^2G_{7/2}^e$	3.813	7.96^{+3}
1296.085	$y^4S_{3/2}^o$	$a^4P_{5/2}^e$	1.670	6.90^{+2}	1475.782	$u^4D_{7/2}^o$	$b^4F_{9/2}^e$	2.805	1.33^{+3}
1296.286	$u^4D_{3/2}^o$	$a^4P_{1/2}^e$	1.723	1.25^{+3}	1490.606	$r^2F_{7/2}^o$	$b^2F_{5/2}^e$	3.943	5.80^{+2}
1298.802	$u^4P_{3/2}^o$	$a^4P_{1/2}^e$	1.723	5.90^{+2}	1494.777	$r^2F_{7/2}^o$	$b^2F_{7/2}^e$	3.966	5.84^{+2}
1299.280	$u^4D_{5/2}^o$	$a^4P_{3/2}^e$	1.695	1.21^{+3}	1497.728	$r^2F_{5/2}^o$	$b^2F_{5/2}^e$	3.943	9.94^{+2}
1299.432	$y^4S_{3/2}^o$	$a^4P_{3/2}^e$	1.695	5.11^{+2}	1508.223	$u^4F_{3/2}^o$	$a^4G_{5/2}^e$	3.229	5.73^{+2}
1299.994	$u^4D_{7/2}^o$	$a^4P_{5/2}^e$	1.670	7.27^{+2}	1534.838	$v^4F_{3/2}^o$	$a^4G_{5/2}^e$	3.229	2.59^{+3}
1301.212	$u^6D_{7/2}^o$	$b^4D_{5/2}^e$	3.890	5.36^{+2}	1536.359	$v^4F_{5/2}^o$	$a^4G_{7/2}^e$	3.220	2.96^{+3}
1308.968	$x^2I_{11/2}^o$	$a^2I_{13/2}^e$	4.074	5.76^{+2}	1538.105	$v^4F_{5/2}^o$	$a^4G_{5/2}^e$	3.229	7.73^{+2}

TABLE 3
FE II FLUXES FOR THE MODEL A WITH Ly α AND Ly β PUMPING.

$\lambda(\text{\AA})$	Upper	Lower	$E_l(\text{eV})$	Flux	$\lambda(\text{\AA})$	Upper	Lower	$E_l(\text{eV})$	Flux
1538.632	$u^4D_{3/2}^o$	$a^4G_{5/2}^e$	3.229	1.77 ⁺³	1723.684	$n^4F_{3/2}^o$	$b^4G_{5/2}^e$	6.727	1.20 ⁺³
1539.045	$v^4F_{7/2}^o$	$a^4G_{9/2}^e$	3.198	4.11 ⁺³	1725.388	$n^4F_{7/2}^o$	$b^4G_{9/2}^e$	6.726	1.60 ⁺³
1539.461	$v^4F_{9/2}^o$	$a^4G_{11/2}^e$	3.151	3.12 ⁺³	1735.681	$n^4F_{9/2}^o$	$b^4G_{11/2}^e$	6.721	1.23 ⁺³
1540.369	$v^4P_{5/2}^o$	$a^4G_{7/2}^e$	3.220	1.28 ⁺³	1739.541	$u^4G_{9/2}^o$	$c^4G_{7/2}^e$	6.220	5.04 ⁺²
1543.234	$v^4F_{7/2}^o$	$a^4G_{7/2}^e$	3.220	1.17 ⁺³	1779.499	$m^4D_{7/2}^o$	$b^4G_{9/2}^e$	6.726	5.03 ⁺²
1547.064	$x^6F_{9/2}^o$	$a^4G_{11/2}^e$	3.151	1.42 ⁺³	1784.891	$n^4F_{5/2}^o$	$b^4G_{7/2}^e$	6.727	1.52 ⁺³
1550.499	$x^6F_{7/2}^o$	$a^4G_{9/2}^e$	3.198	5.37 ⁺²	1785.272	$x^6P_{7/2}^o$	$a^6S_{5/2}^e$	2.890	2.00 ⁺³
1574.497	$t^4P_{1/2}^o$	$b^4D_{1/2}^e$	3.888	5.30 ⁺²	1785.485	$o^4F_{5/2}^o$	$b^4G_{7/2}^e$	6.727	1.25 ⁺³
1577.916	$t^4P_{3/2}^o$	$b^4D_{3/2}^e$	3.887	6.24 ⁺²	1786.753	$x^6P_{5/2}^o$	$a^6S_{5/2}^e$	2.890	1.45 ⁺³
1578.493	$v^2D_{5/2}^o$	$a^2D_{5/2}^e$	2.543	5.19 ⁺²	1787.815	$o^4F_{9/2}^o$	$b^4G_{11/2}^e$	6.721	1.14 ⁺³
1613.942	$t^4F_{3/2}^o$	$b^4D_{1/2}^e$	3.888	6.40 ⁺²	1787.997	$x^6P_{3/2}^o$	$a^6S_{5/2}^e$	2.890	1.23 ⁺³
1633.593	$u^2C_{7/2}^o$	$b^4D_{5/2}^e$	3.890	5.29 ⁺²	1789.844	$o^4F_{7/2}^o$	$b^4G_{9/2}^e$	6.726	1.40 ⁺³
1639.500	$u^4F_{3/2}^o$	$b^4D_{3/2}^e$	3.887	7.48 ⁺²	1793.995	$s^4G_{5/2}^o$	$b^4G_{5/2}^e$	6.727	6.12 ⁺²
1639.606	$u^4F_{3/2}^o$	$b^4D_{1/2}^e$	3.888	1.12 ⁺³	1795.600	$w^2I_{13/2}^o$	$b^4G_{11/2}^e$	6.721	6.43 ⁺²
1640.273	$u^4F_{5/2}^o$	$b^4D_{3/2}^e$	3.887	7.78 ⁺²	1799.316	$s^4G_{9/2}^o$	$b^4G_{9/2}^e$	6.726	1.06 ⁺³
1641.775	$u^4P_{5/2}^o$	$b^4D_{3/2}^e$	3.887	7.12 ⁺²	1799.785	$s^4G_{11/2}^o$	$b^4G_{11/2}^e$	6.721	8.62 ⁺²
1642.183	$u^4F_{7/2}^o$	$b^4D_{5/2}^e$	3.890	5.64 ⁺²	1805.533	$q^4G_{7/2}^o$	$b^4G_{9/2}^e$	6.726	5.61 ⁺²
1671.108	$v^4F_{3/2}^o$	$b^4D_{1/2}^e$	3.888	8.31 ⁺²	1805.719	$v^4D_{5/2}^o$	$b^4D_{5/2}^e$	3.890	6.02 ⁺²
1671.255	$u^4D_{1/2}^o$	$b^4D_{3/2}^e$	3.887	6.06 ⁺²	1805.844	$q^4G_{7/2}^o$	$b^4G_{7/2}^e$	6.727	4.19 ⁺³
1671.654	$v^4F_{3/2}^o$	$b^4D_{5/2}^e$	3.890	1.39 ⁺³	1809.157	$n^4D_{7/2}^o$	$b^4G_{5/2}^e$	6.727	8.05 ⁺²
1674.871	$v^4F_{5/2}^o$	$b^4D_{3/2}^e$	3.887	8.78 ⁺²	1812.266	$v^4D_{3/2}^o$	$b^4D_{3/2}^e$	3.887	5.92 ⁺²
1675.496	$u^4D_{3/2}^o$	$b^4D_{3/2}^e$	3.887	1.39 ⁺³	1813.037	$v^4D_{3/2}^o$	$b^4D_{5/2}^e$	3.890	6.28 ⁺²
1676.155	$u^4D_{3/2}^o$	$b^4D_{5/2}^e$	3.890	1.84 ⁺³	1817.376	$v^4D_{1/2}^o$	$b^4D_{3/2}^e$	3.887	7.52 ⁺²
1678.208	$v^4F_{5/2}^o$	$b^4D_{7/2}^e$	3.902	1.32 ⁺³	1817.507	$v^4D_{1/2}^o$	$b^4D_{1/2}^e$	3.888	6.91 ⁺²
1679.702	$u^4P_{3/2}^o$	$b^4D_{3/2}^e$	3.887	7.14 ⁺²	1820.913	$x^2I_{13/2}^o$	$b^4G_{11/2}^e$	6.721	1.05 ⁺³
1680.300	$v^4P_{5/2}^o$	$b^4D_{5/2}^e$	3.890	7.30 ⁺²	1827.230	$q^4D_{3/2}^o$	$b^4G_{5/2}^e$	6.727	5.16 ⁺²
1681.491	$u^4P_{1/2}^o$	$b^4D_{1/2}^e$	3.888	8.78 ⁺²	1830.464	$v^4H_{7/2}^o$	$b^4G_{5/2}^e$	6.727	8.73 ⁺²
1682.994	$v^4P_{5/2}^o$	$b^4D_{7/2}^e$	3.902	2.73 ⁺³	1831.980	$v^4H_{9/2}^o$	$b^4G_{7/2}^e$	6.727	1.19 ⁺³
1683.709	$v^4F_{7/2}^o$	$b^4D_{5/2}^e$	3.890	1.02 ⁺³	1833.646	$v^4H_{11/2}^o$	$b^4G_{9/2}^e$	6.726	1.39 ⁺³
1687.738	$u^4D_{5/2}^o$	$b^4D_{5/2}^e$	3.890	1.26 ⁺³	1834.964	$v^4H_{13/2}^o$	$b^4G_{11/2}^e$	6.721	1.61 ⁺³
1690.455	$u^4D_{5/2}^o$	$b^4D_{7/2}^e$	3.902	1.23 ⁺³	1839.802	$t^4G_{5/2}^o$	$b^4G_{5/2}^e$	6.727	1.48 ⁺³
1697.370	$u^4D_{7/2}^o$	$b^4D_{7/2}^e$	3.902	5.06 ⁺²	1839.999	$t^4G_{7/2}^o$	$b^4G_{7/2}^e$	6.727	1.32 ⁺³
1697.696	$v^4F_{9/2}^o$	$b^4D_{7/2}^e$	3.902	6.57 ⁺²	1841.710	$t^4G_{9/2}^o$	$b^4G_{9/2}^e$	6.726	2.82 ⁺³
1720.274	$q^4G_{9/2}^o$	$b^4G_{9/2}^e$	6.726	5.70 ⁺²	1843.260	$t^4G_{11/2}^o$	$b^4G_{11/2}^e$	6.721	3.25 ⁺³
1721.737	$v^2D_{5/2}^o$	$b^2P_{3/2}^e$	3.196	5.03 ⁺²	1843.487	$p^4F_{7/2}^o$	$b^4G_{9/2}^e$	6.726	2.78 ⁺³

TABLE 3
FE II FLUXES FOR THE MODEL A WITH Ly α AND Ly β PUMPING.

$\lambda(\text{\AA})$	Upper	Lower	$E_l(\text{eV})$	Flux	$\lambda(\text{\AA})$	Upper	Lower	$E_l(\text{eV})$	Flux
1852.353	$p^4F_{9/2}^o$	$b^4G_{11/2}^e$	6.721	1.14 $^{+3}$	2260.083	$z^4F_{9/2}^o$	$a^6D_{9/2}^e$	0.000	6.95 $^{+3}$
1853.028	$u^6D_{7/2}^o$	$b^4G_{9/2}^e$	6.726	1.91 $^{+3}$	2260.237	$z^4D_{1/2}^o$	$a^6D_{1/2}^e$	0.121	6.09 $^{+2}$
1853.355	$u^6D_{7/2}^o$	$b^4G_{7/2}^e$	6.727	1.22 $^{+3}$	2260.861	$z^4F_{5/2}^o$	$a^6D_{3/2}^e$	0.107	1.56 $^{+3}$
1853.778	$p^4F_{9/2}^o$	$b^4G_{9/2}^e$	6.726	6.54 $^{+2}$	2262.686	$z^4D_{3/2}^o$	$a^6D_{3/2}^e$	0.107	8.07 $^{+2}$
1869.553	$u^4G_{11/2}^o$	$b^4G_{11/2}^e$	6.721	8.36 $^{+3}$	2265.994	$z^4D_{5/2}^o$	$a^6D_{5/2}^e$	0.083	1.20 $^{+3}$
1872.638	$u^4G_{9/2}^o$	$b^4G_{9/2}^e$	6.726	1.27 $^{+4}$	2267.584	$z^4F_{7/2}^o$	$a^6D_{5/2}^e$	0.083	3.17 $^{+3}$
1872.973	$u^4G_{9/2}^o$	$b^4G_{7/2}^e$	6.727	9.86 $^{+2}$	2268.562	$z^4D_{3/2}^o$	$a^6D_{1/2}^e$	0.121	5.93 $^{+2}$
1877.716	$u^4G_{7/2}^o$	$b^4G_{9/2}^e$	6.726	5.18 $^{+2}$	2268.822	$z^4D_{7/2}^o$	$a^6D_{7/2}^e$	0.048	2.31 $^{+3}$
1880.530	$u^6F_{7/2}^o$	$b^4G_{7/2}^e$	6.727	1.41 $^{+3}$	2276.051	$z^4D_{5/2}^o$	$a^6D_{3/2}^e$	0.107	7.73 $^{+2}$
1890.643	$q^4F_{7/2}^o$	$b^4G_{9/2}^e$	6.726	6.29 $^{+2}$	2279.918	$z^4F_{9/2}^o$	$a^6D_{7/2}^e$	0.048	6.81 $^{+3}$
1891.051	$q^4P_{5/2}^o$	$b^4G_{7/2}^e$	6.727	5.76 $^{+2}$	2287.145	$r^2F_{5/2}^o$	$d^2F_{5/2}^e$	6.800	9.78 $^{+2}$
1901.504	$o^4D_{7/2}^o$	$b^4G_{9/2}^e$	6.726	6.91 $^{+2}$	2307.721	$t^4F_{5/2}^o$	$c^4F_{3/2}^e$	6.206	5.68 $^{+2}$
1920.985	$v^2D_{5/2}^o$	$b^2F_{5/2}^e$	3.943	6.05 $^{+2}$	2308.768	$t^4F_{7/2}^o$	$c^4F_{7/2}^e$	6.220	5.98 $^{+2}$
1927.918	$v^2D_{5/2}^o$	$b^2F_{7/2}^e$	3.966	7.93 $^{+2}$	2311.287	$t^4F_{3/2}^o$	$c^4F_{3/2}^e$	6.206	8.17 $^{+2}$
1966.196	$r^2F_{7/2}^o$	$d^2D_{5/2}^e$	5.954	8.63 $^{+2}$	2311.293	$t^4F_{5/2}^o$	$c^4F_{5/2}^e$	6.214	7.52 $^{+2}$
1970.328	$w^4H_{7/2}^o$	$b^4G_{5/2}^e$	6.727	3.14 $^{+3}$	2314.870	$t^4F_{3/2}^o$	$c^4F_{5/2}^e$	6.214	6.10 $^{+2}$
1974.153	$w^4H_{9/2}^o$	$b^4G_{7/2}^e$	6.727	4.15 $^{+3}$	2326.357	$t^4D_{7/2}^o$	$c^4F_{9/2}^e$	6.216	7.47 $^{+2}$
1978.508	$w^4H_{11/2}^o$	$b^4G_{9/2}^e$	6.726	4.24 $^{+3}$	2327.399	$z^6P_{3/2}^o$	$a^6D_{5/2}^e$	0.083	1.88 $^{+3}$
1983.063	$w^4H_{13/2}^o$	$b^4G_{11/2}^e$	6.721	3.76 $^{+3}$	2331.305	$z^4F_{7/2}^o$	$a^4F_{9/2}^e$	0.232	4.67 $^{+3}$
2020.479	$p^4D_{5/2}^o$	$d^4P_{3/2}^e$	7.125	5.10 $^{+2}$	2332.800	$z^6P_{5/2}^o$	$a^6D_{7/2}^e$	0.048	2.61 $^{+3}$
2099.487	$v^2D_{5/2}^o$	$b^2D_{5/2}^e$	4.493	6.92 $^{+2}$	2338.011	$z^6P_{3/2}^o$	$a^6D_{3/2}^e$	0.107	1.91 $^{+3}$
2146.045	$z^4P_{5/2}^o$	$a^6D_{7/2}^e$	0.048	1.20 $^{+3}$	2340.578	$t^4D_{5/2}^o$	$c^4F_{7/2}^e$	6.220	9.98 $^{+2}$
2187.295	$v^2D_{5/2}^o$	$c^2D_{5/2}^e$	4.730	5.62 $^{+2}$	2343.498	$z^6P_{7/2}^o$	$a^6D_{9/2}^e$	0.000	3.18 $^{+3}$
2240.346	$z^4F_{3/2}^o$	$a^6D_{5/2}^e$	0.083	7.65 $^{+2}$	2343.961	$z^4F_{5/2}^o$	$a^4F_{7/2}^e$	0.301	2.52 $^{+3}$
2243.883	$z^4P_{3/2}^o$	$a^4F_{5/2}^e$	0.352	5.13 $^{+2}$	2344.285	$z^6P_{3/2}^o$	$a^6D_{1/2}^e$	0.121	1.90 $^{+3}$
2244.610	$z^4P_{5/2}^o$	$a^4F_{7/2}^e$	0.301	1.46 $^{+3}$	2347.399	$h^4G_{7/2}^e$	$x^4G_{7/2}^o$	8.171	2.11 $^{+3}$
2245.502	$a^6F_{9/2}^e$	$z^6D_{9/2}^o$	4.766	6.39 $^{+2}$	2348.114	$z^4D_{7/2}^o$	$a^4F_{9/2}^e$	0.232	4.99 $^{+3}$
2249.178	$z^4D_{7/2}^o$	$a^6D_{9/2}^e$	0.000	3.56 $^{+3}$	2348.265	$t^4D_{3/2}^o$	$c^4F_{3/2}^e$	6.206	7.09 $^{+2}$
2250.177	$z^4F_{3/2}^o$	$a^6D_{3/2}^e$	0.107	1.11 $^{+3}$	2348.303	$z^6P_{5/2}^o$	$a^6D_{5/2}^e$	0.083	2.65 $^{+3}$
2250.937	$z^4F_{5/2}^o$	$a^6D_{5/2}^e$	0.083	1.70 $^{+3}$	2349.300	$e^4H_{7/2}^e$	$x^4G_{5/2}^o$	8.189	5.59 $^{+2}$
2251.555	$z^4D_{5/2}^o$	$a^6D_{7/2}^e$	0.048	9.87 $^{+2}$	2351.028	$h^4G_{9/2}^e$	$x^4G_{9/2}^o$	8.142	4.02 $^{+3}$
2253.125	$z^4F_{7/2}^o$	$a^6D_{7/2}^e$	0.048	3.56 $^{+3}$	2351.963	$t^4D_{3/2}^o$	$c^4F_{5/2}^e$	6.214	9.05 $^{+2}$
2255.689	$a^6F_{9/2}^e$	$z^6D_{7/2}^o$	4.791	5.46 $^{+2}$	2354.370	$h^4G_{5/2}^e$	$x^4G_{5/2}^o$	8.189	1.35 $^{+3}$
2255.988	$z^4F_{3/2}^o$	$a^6D_{1/2}^e$	0.121	9.48 $^{+2}$	2354.890	$z^4F_{3/2}^o$	$a^4F_{5/2}^e$	0.352	2.12 $^{+3}$
2258.228	$h^4C_{9/2}^e$	$y^4G_{9/2}^o$	7.925	5.45 $^{+2}$	2355.351	$a^6G_{5/2}^e$	$z^6F_{3/2}^o$	5.255	5.42 $^{+2}$

TABLE 3
FE II FLUXES FOR THE MODEL A WITH Ly α AND Ly β PUMPING.

$\lambda(\text{\AA})$	Upper	Lower	$E_l(\text{eV})$	Flux	$\lambda(\text{\AA})$	Upper	Lower	$E_l(\text{eV})$	Flux
2356.941	$u^2 G_{7/2}^o$	$c^4 F_{7/2}^e$	6.220	5.50^{+2}	2384.383	$h^4 G_{5/2}^e$	$x^4 F_{3/2}^o$	8.255	5.14^{+2}
2359.106	$z^6 P_{5/2}^o$	$a^6 D_{3/2}^e$	0.107	2.72^{+3}	2384.385	$z^4 D_{3/2}^o$	$a^4 F_{3/2}^e$	0.386	1.70^{+3}
2359.108	$a^6 G_{7/2}^e$	$z^6 F_{5/2}^o$	5.247	9.48^{+2}	2385.003	$z^4 F_{7/2}^o$	$a^4 F_{5/2}^e$	0.352	3.54^{+3}
2360.001	$z^4 F_{9/2}^o$	$a^4 F_{9/2}^e$	0.232	8.16^{+3}	2386.376	$e^4 F_{9/2}^e$	$z^4 F_{9/2}^o$	5.482	9.60^{+2}
2360.292	$z^4 D_{5/2}^o$	$a^4 F_{7/2}^e$	0.301	2.37^{+3}	2388.631	$z^6 F_{7/2}^o$	$a^6 D_{7/2}^e$	0.048	5.26^{+3}
2361.738	$a^6 G_{11/2}^e$	$z^6 F_{11/2}^o$	5.201	5.96^{+2}	2389.311	$h^4 G_{9/2}^e$	$x^4 F_{7/2}^o$	8.226	1.70^{+3}
2362.018	$z^4 F_{7/2}^o$	$a^4 F_{7/2}^e$	0.301	4.41^{+3}	2391.480	$z^4 F_{9/2}^o$	$a^4 F_{7/2}^e$	0.301	7.02^{+3}
2363.859	$a^6 G_{9/2}^e$	$z^6 F_{7/2}^o$	5.235	2.74^{+3}	2391.739	$u^4 P_{3/2}^o$	$c^4 P_{1/2}^e$	6.085	7.70^{+2}
2364.307	$u^4 F_{3/2}^o$	$c^4 F_{3/2}^e$	6.206	1.16^{+3}	2394.247	$h^4 G_{9/2}^e$	$y^4 H_{11/2}^o$	8.237	5.53^{+2}
2364.831	$z^6 P_{7/2}^o$	$a^6 D_{7/2}^e$	0.048	3.26^{+3}	2395.141	$u^4 P_{1/2}^o$	$c^4 P_{1/2}^e$	6.085	2.07^{+3}
2366.594	$z^4 F_{5/2}^o$	$a^4 F_{5/2}^e$	0.352	2.34^{+3}	2395.421	$z^6 F_{3/2}^o$	$a^6 D_{5/2}^e$	0.083	2.21^{+3}
2368.056	$u^4 F_{3/2}^o$	$c^4 F_{5/2}^e$	6.214	1.08^{+3}	2395.623	$z^6 F_{9/2}^o$	$a^6 D_{7/2}^e$	0.048	9.12^{+3}
2368.593	$z^4 D_{3/2}^o$	$a^4 F_{5/2}^e$	0.352	1.84^{+3}	2397.764	$u^4 D_{1/2}^o$	$c^4 P_{3/2}^e$	6.136	3.26^{+3}
2369.670	$u^4 F_{5/2}^o$	$c^4 F_{5/2}^e$	6.214	8.15^{+2}	2398.654	$e^4 F_{9/2}^e$	$z^4 D_{7/2}^o$	5.508	1.73^{+3}
2369.960	$a^6 G_{11/2}^e$	$z^6 F_{9/2}^o$	5.219	4.73^{+3}	2399.232	$z^4 D_{5/2}^o$	$a^4 F_{3/2}^e$	0.386	1.52^{+3}
2370.499	$z^4 F_{3/2}^o$	$a^4 F_{3/2}^e$	0.386	2.01^{+3}	2399.244	$z^6 F_{5/2}^o$	$a^6 D_{5/2}^e$	0.083	3.75^{+3}
2372.200	$u^4 F_{5/2}^o$	$c^4 F_{7/2}^e$	6.220	1.11^{+3}	2401.291	$e^4 F_{7/2}^e$	$z^4 D_{5/2}^o$	5.550	1.44^{+3}
2372.806	$u^4 P_{5/2}^o$	$c^4 F_{5/2}^e$	6.214	8.96^{+2}	2402.598	$z^4 D_{7/2}^o$	$a^4 F_{5/2}^e$	0.352	3.30^{+3}
2373.158	$u^4 F_{7/2}^o$	$c^4 F_{9/2}^e$	6.216	6.19^{+2}	2404.433	$z^6 F_{1/2}^o$	$a^6 D_{3/2}^e$	0.107	1.80^{+3}
2373.733	$z^6 F_{9/2}^o$	$a^6 D_{9/2}^e$	0.000	1.04^{+4}	2404.888	$z^6 F_{7/2}^o$	$a^6 D_{5/2}^e$	0.083	5.16^{+3}
2374.123	$v^4 F_{3/2}^o$	$c^4 P_{1/2}^e$	6.085	2.10^{+3}	2405.216	$v^4 F_{5/2}^o$	$c^4 P_{3/2}^e$	6.136	7.80^{+2}
2374.643	$u^4 D_{1/2}^o$	$c^4 P_{1/2}^e$	6.085	1.19^{+3}	2405.686	$e^4 F_{5/2}^e$	$z^4 D_{3/2}^o$	5.582	1.02^{+3}
2374.872	$u^4 F_{7/2}^o$	$c^4 F_{7/2}^e$	6.220	7.72^{+2}	2406.663	$z^6 F_{3/2}^o$	$a^6 D_{3/2}^e$	0.107	2.23^{+3}
2375.190	$z^4 D_{1/2}^o$	$a^4 F_{3/2}^e$	0.386	1.34^{+3}	2407.231	$y^4 S_{3/2}^o$	$c^4 P_{1/2}^e$	6.085	8.95^{+2}
2379.274	$z^4 D_{7/2}^o$	$a^4 F_{7/2}^e$	0.301	4.74^{+3}	2408.656	$e^4 F_{3/2}^e$	$z^4 D_{1/2}^o$	5.603	6.22^{+2}
2379.419	$u^2 G_{9/2}^o$	$c^4 F_{9/2}^e$	6.216	5.16^{+2}	2410.522	$z^6 F_{5/2}^o$	$a^6 D_{3/2}^e$	0.107	3.76^{+3}
2380.432	$h^4 G_{7/2}^e$	$x^4 F_{5/2}^o$	8.244	8.83^{+2}	2411.070	$z^6 F_{1/2}^o$	$a^6 D_{1/2}^e$	0.121	1.83^{+3}
2380.765	$z^6 P_{7/2}^o$	$a^6 D_{5/2}^e$	0.083	3.31^{+3}	2413.312	$z^6 F_{3/2}^o$	$a^6 D_{1/2}^e$	0.121	2.24^{+3}
2382.038	$z^6 F_{11/2}^o$	$a^6 D_{9/2}^e$	0.000	3.35^{+4}	2415.061	$v^4 P_{5/2}^o$	$c^4 P_{3/2}^e$	6.136	3.02^{+3}
2382.359	$z^4 F_{5/2}^o$	$a^4 F_{3/2}^e$	0.386	2.06^{+3}	2415.196	$u^4 P_{3/2}^o$	$c^4 P_{3/2}^e$	6.136	9.71^{+2}
2382.568	$t^4 G_{7/2}^o$	$y^4 H_{7/2}^o$	8.263	7.53^{+2}	2416.452	$e^4 F_{9/2}^e$	$z^4 F_{7/2}^o$	5.546	1.09^{+3}
2382.905	$z^2 I_{13/2}^o$	$a^2 H_{11/2}^e$	2.521	7.01^{+2}	2418.434	$e^4 F_{7/2}^e$	$z^4 F_{5/2}^o$	5.587	9.16^{+2}
2383.063	$z^6 F_{5/2}^o$	$a^6 D_{7/2}^e$	0.048	3.76^{+3}	2418.665	$u^4 P_{1/2}^o$	$c^4 P_{3/2}^e$	6.136	3.25^{+3}
2383.216	$u^4 D_{3/2}^o$	$c^4 P_{1/2}^e$	6.085	3.48^{+3}	2424.143	$y^4 G_{11/2}^o$	$b^4 F_{9/2}^e$	2.805	5.68^{+2}
2383.243	$z^4 D_{5/2}^o$	$a^4 F_{5/2}^e$	0.352	2.32^{+3}	2430.397	$v^4 F_{3/2}^o$	$c^4 F_{3/2}^e$	6.206	2.82^{+3}

TABLE 3
FE II FLUXES FOR THE MODEL A WITH Ly α AND Ly β PUMPING.

$\lambda(\text{\AA})$	Upper	Lower	$E_l(\text{eV})$	Flux	$\lambda(\text{\AA})$	Upper	Lower	$E_l(\text{eV})$	Flux
2430.462	$u^4D_{5/2}^o$	$c^4P_{3/2}^e$	6.136	2.85^{+3}	2476.680	$z^6F_{7/2}^o$	$a^4F_{9/2}^e$	0.232	4.18^{+3}
2430.994	$y^4S_{3/2}^o$	$c^4P_{3/2}^e$	6.136	1.02^{+3}	2482.118	$z^4I_{13/2}^o$	$a^4H_{13/2}^e$	2.634	8.35^{+2}
2438.517	$v^4F_{3/2}^o$	$c^4P_{5/2}^e$	6.223	5.14^{+3}	2482.659	$x^4G_{9/2}^o$	$a^4G_{11/2}^e$	3.151	6.57^{+2}
2438.602	$v^4F_{5/2}^o$	$c^4F_{3/2}^e$	6.206	6.01^{+2}	2482.666	$r^2F_{7/2}^o$	$d^2G_{9/2}^e$	7.266	5.34^{+2}
2439.300	$y^4H_{13/2}^o$	$a^4G_{11/2}^e$	3.151	7.22^{+2}	2482.869	$e^4D_{3/2}^e$	$z^4D_{5/2}^o$	5.550	6.22^{+2}
2439.444	$d^4D_{7/2}^e$	$z^6D_{9/2}^o$	4.766	7.05^{+2}	2484.197	$z^6F_{9/2}^o$	$a^4F_{9/2}^e$	0.232	1.21^{+4}
2439.928	$u^4D_{3/2}^o$	$c^4F_{3/2}^e$	6.206	9.69^{+2}	2484.447	$e^4D_{7/2}^e$	$z^4D_{7/2}^o$	5.508	1.95^{+3}
2441.131	$c^4G_{9/2}^e$	$z^4F_{9/2}^o$	5.482	1.02^{+3}	2485.010	$v^4F_{9/2}^o$	$c^4F_{9/2}^e$	6.216	1.75^{+3}
2442.590	$v^4F_{5/2}^o$	$c^4F_{5/2}^e$	6.214	2.43^{+3}	2485.075	$z^6P_{7/2}^o$	$a^4F_{7/2}^e$	0.301	1.48^{+3}
2443.921	$u^4D_{3/2}^o$	$c^4F_{5/2}^e$	6.214	1.85^{+3}	2486.889	$v^4F_{9/2}^o$	$c^4F_{7/2}^e$	6.220	5.48^{+2}
2444.517	$y^4D_{7/2}^o$	$b^4P_{5/2}^e$	2.582	5.77^{+2}	2489.485	$z^4I_{11/2}^o$	$a^4H_{11/2}^e$	2.656	6.22^{+2}
2445.279	$v^4F_{5/2}^o$	$c^4F_{7/2}^e$	6.220	5.02^{+2}	2493.185	$z^4I_{13/2}^o$	$a^4H_{11/2}^e$	2.656	9.06^{+2}
2446.474	$z^2I_{13/2}^o$	$a^4H_{11/2}^e$	2.656	7.88^{+2}	2493.260	$z^4I_{15/2}^o$	$a^4H_{13/2}^e$	2.634	3.06^{+3}
2446.776	$v^4F_{5/2}^o$	$c^4P_{5/2}^e$	6.223	2.75^{+3}	2493.881	$e^4D_{5/2}^e$	$z^4D_{5/2}^o$	5.550	8.14^{+2}
2448.111	$u^4D_{3/2}^o$	$c^4P_{5/2}^e$	6.223	6.08^{+3}	2498.896	$z^4I_{11/2}^o$	$a^4H_{9/2}^e$	2.675	7.60^{+2}
2449.729	$z^6P_{5/2}^o$	$a^4F_{7/2}^e$	0.301	1.26^{+3}	2503.325	$z^2H_{11/2}^o$	$a^4G_{11/2}^e$	3.151	6.23^{+2}
2451.102	$z^6P_{7/2}^o$	$a^4F_{9/2}^e$	0.232	2.08^{+3}	2505.216	$z^6F_{5/2}^o$	$a^4F_{7/2}^e$	0.301	3.14^{+3}
2452.745	$v^4P_{5/2}^o$	$c^4F_{5/2}^e$	6.214	6.30^{+2}	2506.094	$x^4G_{9/2}^o$	$a^4G_{9/2}^e$	3.198	5.58^{+2}
2453.981	$c^4G_{9/2}^e$	$z^4D_{7/2}^o$	5.508	8.86^{+2}	2506.797	$x^6F_{9/2}^o$	$c^4F_{7/2}^e$	6.220	8.81^{+2}
2455.456	$v^4P_{5/2}^o$	$c^4F_{7/2}^e$	6.220	7.74^{+2}	2507.598	$b^6D_{3/2}^e$	$z^6D_{5/2}^o$	4.816	1.28^{+3}
2455.714	$c^4G_{7/2}^e$	$z^4F_{7/2}^o$	5.546	8.99^{+2}	2507.687	$b^6D_{5/2}^e$	$z^6D_{7/2}^o$	4.791	3.56^{+3}
2456.966	$v^4P_{5/2}^o$	$c^4P_{5/2}^e$	6.223	3.80^{+3}	2509.864	$b^6D_{1/2}^e$	$z^6D_{3/2}^o$	4.835	5.20^{+2}
2457.105	$u^4P_{3/2}^o$	$c^4P_{5/2}^e$	6.223	4.06^{+3}	2511.370	$z^6F_{7/2}^o$	$a^4F_{7/2}^e$	0.301	3.88^{+3}
2457.582	$c^4G_{7/2}^e$	$z^4D_{5/2}^o$	5.550	5.27^{+2}	2511.767	$z^4I_{9/2}^o$	$a^4H_{7/2}^e$	2.691	6.26^{+2}
2458.783	$y^4H_{11/2}^o$	$a^4G_{9/2}^e$	3.198	5.26^{+2}	2513.153	$b^6D_{7/2}^e$	$z^6D_{9/2}^o$	4.766	3.87^{+3}
2460.018	$v^4F_{7/2}^o$	$c^4F_{5/2}^e$	6.214	8.46^{+2}	2520.266	$b^6D_{5/2}^e$	$z^6D_{5/2}^o$	4.816	2.29^{+3}
2460.437	$c^4G_{11/2}^e$	$z^4F_{9/2}^o$	5.482	6.31^{+3}	2523.442	$b^6D_{3/2}^e$	$z^6D_{1/2}^o$	4.847	1.19^{+3}
2462.319	$c^4G_{5/2}^e$	$z^4F_{5/2}^o$	5.587	6.50^{+2}	2525.387	$z^4H_{13/2}^o$	$a^4H_{13/2}^e$	2.634	9.22^{+2}
2462.745	$v^4F_{7/2}^o$	$c^4F_{7/2}^e$	6.220	3.05^{+3}	2525.920	$b^6D_{7/2}^e$	$z^6D_{7/2}^o$	4.791	1.11^{+4}
2472.612	$c^4G_{9/2}^e$	$z^4F_{7/2}^o$	5.546	4.36^{+3}	2526.291	$y^4P_{5/2}^o$	$b^4P_{5/2}^e$	2.582	7.79^{+2}
2472.907	$u^4D_{5/2}^o$	$c^4P_{5/2}^e$	6.223	2.84^{+3}	2526.832	$z^6F_{3/2}^o$	$a^4F_{5/2}^e$	0.352	1.16^{+3}
2473.458	$y^4S_{3/2}^o$	$c^4P_{5/2}^e$	6.223	8.96^{+2}	2529.230	$x^4G_{9/2}^o$	$b^2H_{11/2}^e$	3.243	5.74^{+2}
2474.461	$z^6P_{5/2}^o$	$a^4F_{5/2}^e$	0.352	1.02^{+3}	2529.546	$y^4F_{9/2}^o$	$b^4F_{9/2}^e$	2.805	5.37^{+2}
2475.118	$c^4G_{5/2}^e$	$z^4F_{3/2}^o$	5.613	2.50^{+3}	2530.101	$b^6D_{5/2}^e$	$z^6D_{3/2}^o$	4.835	5.93^{+3}
2475.541	$c^4G_{7/2}^e$	$z^4F_{5/2}^o$	5.587	3.09^{+3}	2533.626	$z^4H_{11/2}^o$	$a^4H_{11/2}^e$	2.656	7.60^{+2}

TABLE 3
FE II FLUXES FOR THE MODEL A WITH Ly α AND Ly β PUMPING.

$\lambda(\text{\AA})$	Upper	Lower	$E_l(\text{eV})$	Flux	$\lambda(\text{\AA})$	Upper	Lower	$E_l(\text{eV})$	Flux
2536.844	$z^4 H_{13/2}^o$	$a^4 H_{11/2}^e$	2.656	8.60^{+2}	2669.930	$v^4 D_{3/2}^o$	$c^4 P_{1/2}^e$	6.085	5.70^{+2}
2537.141	$b^6 D_{9/2}^e$	$z^6 D_{9/2}^o$	4.766	3.43^{+3}	2681.041	$v^4 D_{1/2}^o$	$c^4 P_{1/2}^e$	6.085	9.21^{+2}
2538.682	$b^6 D_{7/2}^e$	$z^6 D_{5/2}^o$	4.816	1.09^{+4}	2692.604	$y^2 H_{11/2}^o$	$b^2 G_{9/2}^e$	3.766	5.10^{+2}
2538.993	$z^4 G_{11/2}^o$	$a^4 H_{13/2}^e$	2.634	8.09^{+2}	2692.834	$z^4 F_{5/2}^o$	$a^4 D_{7/2}^e$	0.986	2.56^{+3}
2542.320	$z^6 F_{1/2}^o$	$a^4 F_{3/2}^e$	0.386	7.62^{+2}	2699.194	$v^4 D_{3/2}^o$	$c^4 P_{3/2}^e$	6.136	6.40^{+2}
2543.374	$z^4 H_{11/2}^o$	$a^4 H_{9/2}^e$	2.675	6.08^{+2}	2709.381	$z^4 F_{3/2}^o$	$a^4 D_{5/2}^e$	1.040	1.83^{+3}
2550.153	$b^6 D_{9/2}^e$	$z^6 D_{7/2}^o$	4.791	1.20^{+3}	2710.550	$v^4 D_{1/2}^o$	$c^4 P_{3/2}^e$	6.136	9.54^{+2}
2562.535	$z^4 P_{5/2}^o$	$a^4 D_{7/2}^e$	0.986	3.64^{+3}	2711.841	$z^2 I_{13/2}^o$	$a^4 G_{11/2}^e$	3.151	1.07^{+3}
2563.479	$z^4 P_{3/2}^o$	$a^4 D_{5/2}^e$	1.040	1.99^{+3}	2714.411	$z^4 D_{5/2}^o$	$a^4 D_{7/2}^e$	0.986	2.72^{+3}
2566.911	$z^4 P_{1/2}^o$	$a^4 D_{3/2}^e$	1.076	1.64^{+3}	2716.564	$d^2 H_{11/2}^e$	$z^2 I_{13/2}^o$	7.720	7.53^{+2}
2574.368	$z^4 S_{3/2}^o$	$b^4 P_{5/2}^e$	2.582	8.30^{+2}	2716.694	$z^4 F_{7/2}^o$	$a^4 D_{7/2}^e$	0.986	2.62^{+3}
2577.921	$z^4 P_{1/2}^o$	$a^4 D_{1/2}^e$	1.096	1.64^{+3}	2717.520	$v^4 F_{5/2}^o$	$b^4 G_{7/2}^e$	6.727	8.12^{+2}
2579.120	$a^4 S_{3/2}^e$	$z^4 P_{5/2}^o$	5.821	7.86^{+2}	2717.966	$d^4 D_{7/2}^e$	$z^6 P_{7/2}^o$	5.287	2.00^{+3}
2582.587	$z^4 P_{3/2}^o$	$a^4 D_{3/2}^e$	1.076	1.89^{+3}	2718.640	$v^4 D_{7/2}^o$	$c^4 F_{9/2}^e$	6.216	1.10^{+3}
2585.878	$z^6 D_{7/2}^o$	$a^6 D_{9/2}^e$	0.000	1.21^{+4}	2720.889	$v^4 D_{7/2}^o$	$c^4 F_{7/2}^e$	6.220	6.17^{+2}
2591.543	$z^4 P_{5/2}^o$	$a^4 D_{5/2}^e$	1.040	3.88^{+3}	2724.885	$z^4 F_{5/2}^o$	$a^4 D_{5/2}^e$	1.040	3.30^{+3}
2592.782	$z^2 K_{15/2}^o$	$a^2 I_{13/2}^e$	4.074	7.31^{+2}	2727.537	$z^4 D_{3/2}^o$	$a^4 D_{5/2}^e$	1.040	2.31^{+3}
2593.732	$z^4 P_{3/2}^o$	$a^4 D_{1/2}^e$	1.096	1.62^{+3}	2727.937	$d^4 D_{5/2}^e$	$z^6 P_{5/2}^o$	5.359	6.39^{+2}
2598.369	$z^6 D_{5/2}^o$	$a^6 D_{7/2}^e$	0.048	7.46^{+3}	2729.588	$v^4 D_{5/2}^o$	$c^4 F_{5/2}^e$	6.214	9.49^{+2}
2599.396	$z^6 D_{9/2}^o$	$a^6 D_{9/2}^e$	0.000	1.38^{+4}	2730.735	$z^4 F_{3/2}^o$	$a^4 D_{3/2}^e$	1.076	2.83^{+3}
2607.091	$z^6 D_{3/2}^o$	$a^6 D_{5/2}^e$	0.083	5.30^{+3}	2732.446	$z^6 D_{9/2}^o$	$a^4 F_{9/2}^e$	0.232	1.12^{+4}
2611.072	$z^4 P_{5/2}^o$	$a^4 D_{3/2}^e$	1.076	3.52^{+3}	2732.946	$v^4 D_{5/2}^o$	$c^4 F_{7/2}^e$	6.220	1.36^{+3}
2611.876	$z^6 D_{7/2}^o$	$a^6 D_{7/2}^e$	0.048	1.19^{+4}	2736.962	$z^4 D_{1/2}^o$	$a^4 D_{3/2}^e$	1.076	1.64^{+3}
2613.826	$z^6 D_{1/2}^o$	$a^6 D_{3/2}^e$	0.107	4.09^{+3}	2738.393	$v^4 F_{7/2}^o$	$b^4 G_{9/2}^e$	6.726	1.68^{+3}
2617.617	$z^6 D_{5/2}^o$	$a^6 D_{5/2}^e$	0.083	8.15^{+3}	2739.546	$z^4 D_{7/2}^o$	$a^4 D_{7/2}^e$	0.986	5.61^{+3}
2620.413	$z^6 D_{3/2}^o$	$a^6 D_{3/2}^e$	0.107	4.66^{+3}	2741.310	$v^4 D_{3/2}^o$	$c^4 F_{3/2}^e$	6.206	1.34^{+3}
2621.671	$z^6 D_{1/2}^o$	$a^6 D_{1/2}^e$	0.121	4.26^{+3}	2743.198	$z^4 F_{3/2}^o$	$a^4 D_{1/2}^e$	1.096	2.83^{+3}
2625.059	$u^4 F_{3/2}^o$	$b^4 G_{5/2}^e$	6.727	7.51^{+2}	2743.225	$b^6 D_{1/2}^e$	$z^6 F_{3/2}^o$	5.255	5.11^{+2}
2625.490	$z^2 K_{13/2}^o$	$a^2 I_{11/2}^e$	4.079	5.52^{+2}	2746.128	$b^6 D_{1/2}^e$	$z^6 F_{1/2}^o$	5.260	5.96^{+2}
2625.668	$z^6 D_{9/2}^o$	$a^6 D_{7/2}^e$	0.048	1.62^{+4}	2746.351	$v^4 D_{3/2}^o$	$c^4 F_{5/2}^e$	6.214	1.83^{+3}
2628.298	$z^6 D_{3/2}^o$	$a^6 D_{1/2}^e$	0.121	5.48^{+3}	2746.484	$z^4 F_{5/2}^o$	$a^4 D_{3/2}^e$	1.076	3.15^{+3}
2631.047	$z^6 D_{5/2}^o$	$a^6 D_{3/2}^e$	0.107	7.84^{+3}	2746.981	$z^4 D_{5/2}^o$	$a^4 D_{5/2}^e$	1.040	2.95^{+3}
2631.325	$z^6 D_{7/2}^o$	$a^6 D_{5/2}^e$	0.083	1.28^{+4}	2747.121	$b^6 D_{3/2}^o$	$z^6 F_{5/2}^o$	5.247	2.04^{+3}
2631.604	$z^4 G_{11/2}^o$	$b^4 F_{9/2}^e$	2.805	7.20^{+2}	2749.178	$z^4 D_{3/2}^o$	$a^4 D_{3/2}^e$	1.076	2.26^{+3}
2650.486	$e^4 D_{7/2}^e$	$z^4 P_{5/2}^o$	5.821	1.28^{+3}	2749.319	$z^4 F_{7/2}^o$	$a^4 D_{5/2}^e$	1.040	5.90^{+3}

TABLE 3
FE II FLUXES FOR THE MODEL A WITH Ly α AND Ly β PUMPING.

$\lambda(\text{\AA})$	Upper	Lower	$E_l(\text{eV})$	Flux	$\lambda(\text{\AA})$	Upper	Lower	$E_l(\text{eV})$	Flux
2749.482	$z^4D_{1/2}^o$	$a^4D_{1/2}^e$	1.096	1.61^{+3}	2858.629	$d^4D_{3/2}^e$	$z^4D_{1/2}^o$	5.603	6.99^{+3}
2749.484	$u^2F_{5/2}^o$	$c^4F_{7/2}^e$	6.220	8.87^{+2}	2861.171	$z^6P_{3/2}^o$	$a^4D_{3/2}^e$	1.076	9.60^{+2}
2752.151	$b^6D_{3/2}^e$	$z^6F_{3/2}^o$	5.255	1.50^{+3}	2864.121	$b^6D_{5/2}^e$	$z^6P_{3/2}^o$	5.406	1.71^{+3}
2753.024	$v^4D_{1/2}^o$	$c^4F_{3/2}^e$	6.206	2.46^{+3}	2865.454	$d^4D_{3/2}^e$	$z^4F_{3/2}^o$	5.613	4.55^{+3}
2753.291	$z^2I_{11/2}^o$	$b^2H_{9/2}^e$	3.266	6.06^{+2}	2868.875	$z^6P_{5/2}^o$	$a^4D_{5/2}^e$	1.040	2.34^{+3}
2754.889	$b^6D_{5/2}^e$	$z^6F_{7/2}^o$	5.235	7.35^{+3}	2869.317	$d^4D_{5/2}^e$	$z^4D_{3/2}^o$	5.582	1.02^{+4}
2755.739	$z^4F_{9/2}^o$	$a^4D_{7/2}^e$	0.986	8.92^{+3}	2872.258	$d^4D_{5/2}^e$	$z^4F_{5/2}^o$	5.587	3.49^{+3}
2761.811	$z^4D_{3/2}^o$	$a^4D_{1/2}^e$	1.096	1.97^{+3}	2874.856	$z^6P_{3/2}^o$	$a^4D_{1/2}^e$	1.096	8.53^{+2}
2762.332	$b^6D_{5/2}^e$	$z^6F_{5/2}^o$	5.247	3.27^{+3}	2880.759	$z^6P_{7/2}^o$	$a^4D_{7/2}^e$	0.986	3.45^{+3}
2765.099	$v^4F_{9/2}^o$	$b^4C_{11/2}^e$	6.721	1.60^{+3}	2882.190	$d^4D_{7/2}^e$	$z^4F_{7/2}^o$	5.546	8.76^{+2}
2767.418	$b^6D_{5/2}^e$	$z^6F_{3/2}^o$	5.255	6.68^{+2}	2883.705	$z^4H_{13/2}^o$	$b^2H_{11/2}^e$	3.243	6.35^{+2}
2767.502	$z^2I_{13/2}^o$	$b^2H_{11/2}^e$	3.243	1.15^{+3}	2884.764	$d^4D_{7/2}^e$	$z^4D_{5/2}^o$	5.550	6.86^{+3}
2767.519	$b^6D_{7/2}^e$	$z^6F_{9/2}^o$	5.219	2.02^{+4}	2892.827	$z^6P_{5/2}^o$	$a^4D_{3/2}^e$	1.076	2.08^{+3}
2768.933	$z^4D_{5/2}^o$	$a^4D_{3/2}^e$	1.076	2.26^{+3}	2907.859	$z^6F_{5/2}^o$	$a^4D_{7/2}^e$	0.986	5.24^{+3}
2769.353	$z^4I_{13/2}^o$	$a^4G_{11/2}^e$	3.151	6.96^{+2}	2917.470	$z^6P_{7/2}^o$	$a^4D_{5/2}^e$	1.040	2.67^{+3}
2776.909	$b^6D_{7/2}^e$	$z^6F_{7/2}^o$	5.235	5.58^{+3}	2922.027	$x^4G_{9/2}^o$	$b^4D_{7/2}^e$	3.902	6.12^{+2}
2785.195	$b^6D_{9/2}^e$	$z^6F_{11/2}^o$	5.201	1.44^{+3}	2926.580	$z^6F_{9/2}^o$	$a^4D_{7/2}^e$	0.986	2.14^{+4}
2787.240	$b^6D_{5/2}^e$	$z^6P_{7/2}^o$	5.287	1.15^{+3}	2939.508	$z^6F_{3/2}^o$	$a^4D_{5/2}^e$	1.040	1.62^{+3}
2789.733	$x^6F_{9/2}^o$	$b^4G_{11/2}^e$	6.721	5.65^{+2}	2944.392	$z^4P_{1/2}^o$	$a^4P_{3/2}^e$	1.695	2.04^{+3}
2809.782	$b^6D_{7/2}^e$	$z^6P_{11/2}^o$	5.287	2.98^{+3}	2947.660	$z^4P_{3/2}^o$	$a^4P_{5/2}^e$	1.670	2.10^{+3}
2820.954	$d^4D_{5/2}^e$	$z^4D_{7/2}^o$	5.508	8.62^{+2}	2953.777	$z^6F_{7/2}^o$	$a^4D_{5/2}^e$	1.040	7.96^{+3}
2824.566	$d^4D_{3/2}^e$	$z^4D_{5/2}^o$	5.550	2.98^{+3}	2961.277	$z^6F_{1/2}^o$	$a^4D_{3/2}^e$	1.076	1.42^{+3}
2831.881	$d^4D_{1/2}^e$	$z^4D_{3/2}^o$	5.582	2.83^{+3}	2964.620	$z^4P_{1/2}^o$	$a^4P_{1/2}^e$	1.723	2.11^{+3}
2833.087	$b^6D_{5/2}^e$	$z^6P_{5/2}^o$	5.359	2.35^{+3}	2964.659	$z^6F_{3/2}^o$	$a^4D_{3/2}^e$	1.076	1.60^{+3}
2839.507	$d^4D_{7/2}^e$	$z^4F_{9/2}^o$	5.482	4.77^{+4}	2965.035	$z^4P_{3/2}^o$	$a^4P_{3/2}^e$	1.695	2.05^{+3}
2839.800	$b^6D_{9/2}^e$	$z^6P_{7/2}^o$	5.287	1.25^{+3}	2970.518	$z^6F_{5/2}^o$	$a^4D_{3/2}^e$	1.076	6.05^{+3}
2844.961	$d^4D_{1/2}^e$	$z^4D_{1/2}^o$	5.603	4.14^{+3}	2975.939	$z^6F_{1/2}^o$	$a^4D_{1/2}^e$	1.096	1.46^{+3}
2845.423	$d^4D_{3/2}^e$	$z^4D_{3/2}^o$	5.582	1.29^{+4}	2979.355	$z^6F_{3/2}^o$	$a^4D_{1/2}^e$	1.096	2.12^{+3}
2845.601	$d^4D_{5/2}^e$	$z^4F_{7/2}^o$	5.546	4.80^{+4}	2984.824	$z^4P_{5/2}^o$	$a^4P_{5/2}^e$	1.670	4.61^{+3}
2847.772	$b^6D_{3/2}^e$	$z^6P_{3/2}^o$	5.406	6.46^{+2}	2985.089	$v^4P_{5/2}^o$	$d^4P_{5/2}^e$	7.115	5.60^{+2}
2848.110	$d^4D_{5/2}^e$	$z^4D_{5/2}^o$	5.550	2.16^{+4}	2985.294	$u^4P_{3/2}^o$	$d^4P_{5/2}^e$	7.115	1.63^{+3}
2848.315	$d^4D_{3/2}^e$	$z^4F_{5/2}^o$	5.587	2.39^{+4}	2985.548	$z^4P_{3/2}^o$	$a^4P_{1/2}^e$	1.723	2.16^{+3}
2851.721	$d^4D_{1/2}^e$	$z^4F_{3/2}^o$	5.613	1.79^{+4}	3002.642	$z^4P_{5/2}^o$	$a^4P_{3/2}^e$	1.695	4.82^{+3}
2856.380	$b^6D_{7/2}^e$	$z^6P_{5/2}^o$	5.359	4.93^{+3}	3010.212	$d^4D_{3/2}^e$	$z^4P_{5/2}^o$	5.821	9.70^{+2}
2856.908	$d^4D_{7/2}^e$	$z^4D_{7/2}^o$	5.508	4.25^{+4}	3016.122	$u^4D_{5/2}^o$	$d^4P_{3/2}^e$	7.125	5.03^{+2}

TABLE 3
FE II FLUXES FOR THE MODEL A WITH Ly α AND Ly β PUMPING.

$\lambda(\text{\AA})$	Upper	Lower	$E_l(\text{eV})$	Flux	$\lambda(\text{\AA})$	Upper	Lower	$E_l(\text{eV})$	Flux
3033.437	$d^4D_{1/2}^e$	$z^4P_{3/2}^o$	5.873	1.10^{+3}	3945.214	$z^6D_{3/2}^o$	$a^4P_{3/2}^e$	1.695	4.96^{+3}
3036.967	$d^4D_{5/2}^e$	$z^4P_{5/2}^o$	5.821	4.62^{+3}	4002.098	$z^4P_{3/2}^o$	$b^4P_{1/2}^e$	2.777	1.00^{+3}
3048.981	$d^4D_{3/2}^e$	$z^4P_{3/2}^o$	5.873	5.70^{+3}	4173.452	$z^4D_{5/2}^o$	$b^4P_{5/2}^e$	2.582	4.08^{+3}
3055.352	$d^4D_{1/2}^e$	$z^4P_{1/2}^o$	5.902	4.66^{+3}	4178.850	$z^4F_{7/2}^o$	$b^4P_{5/2}^e$	2.582	7.65^{+3}
3071.122	$d^4D_{3/2}^e$	$z^4P_{1/2}^o$	5.902	3.84^{+3}	4233.163	$z^4D_{7/2}^o$	$b^4P_{5/2}^e$	2.582	9.99^{+3}
3076.432	$d^4D_{5/2}^e$	$z^4P_{3/2}^o$	5.873	7.97^{+3}	4258.153	$z^4F_{3/2}^o$	$b^4P_{3/2}^e$	2.703	2.13^{+3}
3078.678	$d^4D_{5/2}^e$	$z^4P_{5/2}^o$	5.821	1.90^{+4}	4273.314	$z^4D_{1/2}^o$	$b^4P_{3/2}^e$	2.703	1.08^{+3}
3161.976	$z^4F_{3/2}^o$	$a^4P_{3/2}^e$	1.695	2.76^{+3}	4296.572	$z^4F_{5/2}^o$	$b^4P_{3/2}^e$	2.703	4.49^{+3}
3163.096	$z^4F_{5/2}^o$	$a^4P_{5/2}^e$	1.670	3.53^{+3}	4303.168	$z^4D_{3/2}^o$	$b^4P_{3/2}^e$	2.703	3.29^{+3}
3166.670	$z^4D_{3/2}^o$	$a^4P_{5/2}^e$	1.670	1.59^{+3}	4351.762	$z^4D_{5/2}^o$	$b^4P_{3/2}^e$	2.703	4.34^{+3}
3170.329	$z^4D_{1/2}^o$	$a^4P_{3/2}^e$	1.695	1.46^{+3}	4369.420	$z^4F_{3/2}^o$	$b^4P_{1/2}^e$	2.777	1.23^{+3}
3183.112	$z^4F_{5/2}^o$	$a^4P_{3/2}^e$	1.695	4.13^{+3}	4385.385	$z^4D_{1/2}^o$	$b^4P_{1/2}^e$	2.777	2.47^{+3}
3185.316	$z^4F_{3/2}^o$	$a^4P_{1/2}^e$	1.723	3.06^{+3}	4416.831	$z^4D_{3/2}^o$	$b^4P_{1/2}^e$	2.777	3.12^{+3}
3186.731	$z^4D_{3/2}^o$	$a^4P_{3/2}^e$	1.695	2.28^{+3}	4489.179	$z^4F_{5/2}^o$	$b^4F_{7/2}^e$	2.827	4.42^{+3}
3192.908	$z^4D_{5/2}^o$	$a^4P_{5/2}^e$	1.670	2.55^{+3}	4491.414	$z^4F_{3/2}^o$	$b^4F_{3/2}^e$	2.854	4.76^{+3}
3193.792	$z^4D_{1/2}^o$	$a^4P_{1/2}^e$	1.723	1.71^{+3}	4508.284	$z^4D_{1/2}^o$	$b^4F_{3/2}^e$	2.854	2.78^{+3}
3196.067	$z^4F_{7/2}^o$	$a^4P_{5/2}^e$	1.670	5.90^{+3}	4515.345	$z^4F_{5/2}^o$	$b^4F_{5/2}^e$	2.843	6.50^{+3}
3210.439	$z^4D_{3/2}^o$	$a^4P_{1/2}^e$	1.723	2.30^{+3}	4520.207	$z^4F_{7/2}^o$	$b^4F_{9/2}^e$	2.805	7.02^{+3}
3213.304	$z^4D_{5/2}^o$	$a^4P_{3/2}^e$	1.695	2.91^{+3}	4522.631	$z^4D_{3/2}^o$	$b^4F_{5/2}^e$	2.843	3.78^{+3}
3227.741	$z^4D_{7/2}^o$	$a^4P_{5/2}^e$	1.670	6.72^{+3}	4541.524	$z^4D_{3/2}^o$	$b^4F_{3/2}^e$	2.854	1.96^{+3}
3255.889	$z^6D_{7/2}^o$	$a^4D_{7/2}^e$	0.986	2.59^{+4}	4549.462	$z^4D_{5/2}^o$	$b^4F_{7/2}^e$	2.827	4.51^{+3}
3277.348	$z^6D_{9/2}^o$	$a^4D_{7/2}^e$	0.986	2.25^{+4}	4555.878	$z^4F_{7/2}^o$	$b^4F_{7/2}^e$	2.827	8.37^{+3}
3281.291	$z^6D_{5/2}^o$	$a^4D_{5/2}^e$	1.040	1.01^{+4}	4576.339	$z^4D_{5/2}^o$	$b^4F_{5/2}^e$	2.843	2.36^{+3}
3295.823	$z^6D_{3/2}^o$	$a^4D_{3/2}^e$	1.076	4.09^{+3}	4582.831	$z^4F_{7/2}^o$	$b^4F_{5/2}^e$	2.843	4.38^{+3}
3303.467	$z^6D_{1/2}^o$	$a^4D_{1/2}^e$	1.096	5.38^{+3}	4583.822	$z^4D_{7/2}^o$	$b^4F_{9/2}^e$	2.805	1.02^{+4}
3416.011	$z^4P_{1/2}^o$	$a^2P_{3/2}^e$	2.275	2.37^{+3}	4629.337	$z^4F_{9/2}^o$	$b^4F_{9/2}^e$	2.805	1.95^{+4}
3443.827	$z^4P_{3/2}^o$	$a^2P_{3/2}^e$	2.275	1.52^{+3}	4923.941	$z^6P_{3/2}^o$	$a^6S_{5/2}^e$	2.890	2.88^{+3}
3494.664	$z^4P_{5/2}^o$	$a^2P_{3/2}^e$	2.275	4.96^{+3}	5018.443	$z^6P_{5/2}^o$	$a^6S_{5/2}^e$	2.890	5.33^{+3}
3507.405	$z^4P_{3/2}^o$	$a^2P_{1/2}^e$	2.341	1.42^{+3}	5169.046	$z^6P_{7/2}^o$	$a^6S_{5/2}^e$	2.890	5.97^{+3}
3508.202	$z^6F_{3/2}^o$	$a^4P_{1/2}^e$	1.723	2.27^{+3}	5197.593	$z^4F_{3/2}^o$	$a^4G_{5/2}^e$	3.229	6.56^{+3}
3764.108	$z^4P_{3/2}^o$	$b^4P_{5/2}^e$	2.582	2.05^{+3}	5234.626	$z^4F_{5/2}^o$	$a^4G_{7/2}^e$	3.220	7.92^{+3}
3783.336	$z^4D_{5/2}^o$	$a^2P_{3/2}^e$	2.275	2.32^{+3}	5264.818	$z^4D_{3/2}^o$	$a^4G_{5/2}^e$	3.229	1.21^{+3}
3872.761	$z^4P_{1/2}^o$	$b^4P_{3/2}^e$	2.703	1.61^{+3}	5275.977	$z^4F_{7/2}^o$	$a^4G_{9/2}^e$	3.198	9.70^{+3}
3914.513	$z^6D_{3/2}^o$	$a^4P_{5/2}^e$	1.670	5.30^{+3}	5284.117	$z^6F_{7/2}^o$	$a^6S_{5/2}^e$	2.890	8.04^{+3}
3938.290	$z^6D_{5/2}^o$	$a^4P_{5/2}^e$	1.670	1.44^{+4}	5316.621	$z^4F_{9/2}^o$	$a^4G_{11/2}^e$	3.151	2.33^{+4}

TABLE 3
FE II FLUXES FOR THE MODEL A WITH Ly α AND Ly β PUMPING.

$\lambda(\text{\AA})$	Upper	Lower	$E_l(\text{eV})$	Flux	$\lambda(\text{\AA})$	Upper	Lower	$E_l(\text{eV})$	Flux
5316.776	$z^4D_{5/2}^o$	$a^4G_{7/2}^e$	3.220	2.29^{+3}	9210.938	$u^4D_{1/2}^o$	$d^4D_{1/2}^e$	9.957	1.96^{+3}
5325.541	$z^4F_{7/2}^o$	$a^4G_{7/2}^e$	3.220	6.64^{+3}	9296.851	$u^4D_{5/2}^o$	$d^4D_{5/2}^e$	9.900	2.47^{+3}
5362.847	$z^4D_{7/2}^o$	$a^4G_{9/2}^e$	3.198	6.91^{+3}	9325.115	$u^4P_{3/2}^o$	$d^4D_{3/2}^e$	9.937	8.83^{+2}
6147.738	$z^4P_{1/2}^o$	$b^4D_{3/2}^e$	3.887	1.65^{+3}	9377.042	$u^4P_{1/2}^o$	$d^4D_{3/2}^e$	9.937	1.35^{+3}
6149.232	$z^4P_{1/2}^o$	$b^4D_{1/2}^e$	3.888	1.19^{+3}	9406.669	$x^6F_{9/2}^o$	$d^4D_{7/2}^e$	9.845	2.96^{+3}
6238.419	$z^4P_{3/2}^o$	$b^4D_{3/2}^e$	3.887	1.62^{+3}	9572.625	$d^4P_{5/2}^e$	$z^4P_{5/2}^o$	5.821	2.12^{+3}
6247.574	$z^4P_{3/2}^o$	$b^4D_{5/2}^e$	3.890	1.94^{+3}	9812.027	$d^4P_{1/2}^e$	$z^4P_{3/2}^o$	5.873	8.87^{+2}
6317.982	$c^4D_{7/2}^e$	$z^4D_{7/2}^o$	5.508	5.81^{+2}	9956.255	$b^4G_{9/2}^e$	$z^4F_{9/2}^o$	5.482	8.40^{+2}
6416.911	$z^4P_{5/2}^o$	$b^4D_{5/2}^e$	3.890	2.83^{+3}	9997.556	$b^4G_{11/2}^e$	$z^4F_{9/2}^o$	5.482	5.66^{+3}
6456.385	$z^4P_{5/2}^o$	$b^4D_{7/2}^e$	3.902	6.24^{+3}	10131.759	$d^4P_{3/2}^e$	$z^4P_{1/2}^o$	5.902	1.54^{+3}
7308.065	$z^4D_{3/2}^o$	$b^4D_{3/2}^e$	3.887	7.05^{+2}	10173.509	$b^4G_{9/2}^e$	$z^4D_{7/2}^o$	5.508	6.56^{+2}
7462.391	$z^4D_{5/2}^o$	$b^4D_{5/2}^e$	3.890	1.37^{+3}	10491.000	$b^4G_{7/2}^e$	$z^4F_{7/2}^o$	5.546	7.56^{+2}
7711.720	$z^4D_{7/2}^o$	$b^4D_{7/2}^e$	3.902	3.09^{+3}	10501.521	$b^4G_{9/2}^e$	$z^4F_{7/2}^o$	5.546	6.59^{+3}
7970.398	$v^4F_{7/2}^o$	$b^6D_{7/2}^e$	9.696	7.18^{+2}	10862.646	$b^4G_{7/2}^e$	$z^4F_{5/2}^o$	5.587	4.08^{+3}
7981.850	$v^4F_{9/2}^o$	$b^6D_{9/2}^e$	9.650	9.62^{+2}	11125.573	$b^4G_{5/2}^e$	$z^4F_{3/2}^o$	5.613	2.23^{+3}
8157.529	$v^4F_{7/2}^o$	$b^6D_{5/2}^e$	9.732	1.20^{+3}	17324.679	$x^6F_{9/2}^o$	$a^6G_{11/2}^e$	10.447	6.12^{+2}
8190.607	$x^6F_{9/2}^o$	$b^6D_{9/2}^e$	9.650	1.00^{+3}	17865.205	$v^4F_{7/2}^o$	$c^4G_{9/2}^e$	10.557	7.83^{+2}
8228.930	$v^4F_{9/2}^o$	$b^6D_{7/2}^e$	9.696	4.60^{+3}					
8287.545	$x^6F_{7/2}^o$	$b^6D_{7/2}^e$	9.696	1.77^{+3}					
8357.184	$x^6F_{5/2}^o$	$b^6D_{5/2}^e$	9.732	8.22^{+2}					
8420.526	$u^4D_{7/2}^o$	$b^6D_{5/2}^e$	9.732	6.75^{+2}					
8450.990	$x^6F_{9/2}^o$	$b^6D_{7/2}^e$	9.696	1.16^{+4}					
8490.054	$x^6F_{7/2}^o$	$b^6D_{5/2}^e$	9.732	5.56^{+3}					
8499.559	$x^6F_{5/2}^o$	$b^6D_{3/2}^e$	9.757	1.20^{+3}					
8722.372	$v^4P_{5/2}^o$	$d^4D_{7/2}^e$	9.845	1.66^{+3}					
8926.638	$u^4D_{5/2}^o$	$d^4D_{7/2}^e$	9.845	8.68^{+3}					
9075.501	$v^4P_{5/2}^o$	$d^4D_{5/2}^e$	9.900	6.80^{+3}					
9077.400	$u^4P_{3/2}^o$	$d^4D_{5/2}^e$	9.900	4.44^{+3}					
9122.942	$u^4D_{7/2}^o$	$d^4D_{7/2}^e$	9.845	1.19^{+4}					
9132.362	$v^4F_{9/2}^o$	$d^4D_{7/2}^e$	9.845	1.33^{+4}					
9175.869	$v^4F_{7/2}^o$	$d^4D_{5/2}^e$	9.900	1.66^{+4}					
9178.088	$v^4F_{5/2}^o$	$d^4D_{3/2}^e$	9.937	1.15^{+4}					
9196.897	$u^4D_{3/2}^o$	$d^4D_{3/2}^e$	9.937	5.24^{+3}					
9203.122	$v^4F_{3/2}^o$	$d^4D_{1/2}^e$	9.957	7.44^{+3}					
9204.610	$x^6F_{7/2}^o$	$d^4D_{7/2}^e$	9.845	5.38^{+2}					